

A NOVEL APPROACH TO ACTUATOR DISK MODELING

Aviv Rosen¹, and Ohad Gur²

¹ Technion Israel Institute of Technology
Haifa 32000, Israel
e-mail: rosen@aerodyne.technion.ac.il

² Technion Israel Institute of Technology
Haifa 32000, Israel
e-mail: ohadg@aerodyne.technion.ac.il

Key words: Actuator disk, Blade element, Momentum, Axial flow, Hover

Abstract: Actuator disk models are commonly used for the analysis of rotary wing systems. The blade-element momentum model is probably the most popular one because of its simplicity, efficiency and good accuracy in many cases. Yet, momentum models fail to give satisfactory results in many other cases. The reason is probably the fact that momentum models include a basic assumption that the integral form of the equation of conservation of momentum can be replaced by its differential form. The paper presents a new actuator disk model that does not include the above mentioned assumption. It is assumed that the pressure difference between both sides of a certain point of the disk is a time average of the pressure difference between both sides of the blade-elements that pass through that point. In addition to calculating the axial components of the induced velocity through the disk, the new model includes also calculations of the radial component. The analysis of the wake is identical to that of the general momentum theory.

The new model includes an iterative solution procedure which is usually stable and converges relatively fast. The new model is efficient and requires relatively small computing resource and short computing time. The results of the new model are compared with the results of exact actuator disk model, which includes a solution of the entire flow field. Good agreement is shown between the results of both models. The comparisons include the induced velocities through the disk and the induced velocities in the far wake. The results of the new model also exhibit good agreement with test results of a hovering rotor model with different number of blades, and various pitch angles. Increasing differences are shown between these test results and the calculations of the general momentum model.

1 INTRODUCTION

The first models that were used to analyze rotary-wings were actuator disk models that were suggested by Rankin and Froud ^[1] for the analysis of marine propellers. According to actuator disk models, the propeller or rotor are replaced by an artificial thin disk that produces sudden discontinuities of the flow properties. In spite of the development of more sophisticated models during the years, that includes: prescribed wake models, free wake models and various CFD models – actuator disk models are probably the most popular for the analysis of rotary wing systems because of their simplicity and efficiency on one hand, and the relative good accuracy that they offer on the other hand.

Horlock ^[2] presents an excellent overview of the principles of various actuator disk models and their application to various problems. In what follows, only a brief review will be presented, that is important in order to understand the advantages of the new model that will be presented in the paper.

The best known, and probably more popular than any other model, is the actuator disk model associated with the Momentum theory ^[3]. It is based on applying the basics principles of conservation of mass, momentum and energy. The complete model is known as the general momentum model. There also exist different simplified momentum models. Yet, this model has a major weakness: the integral representing the conservation of axial momentum, is replaced by its differential form. Glauert ^[3] indicated that: “the validity of this equation has not been established and its adoption may imply the neglect of the mutual interference between the various annular elements of the propeller, but the actual deviations from the conditions presented by ... are believed to be extremely small in general.” The adoption of this assumption may be one of the reasons to the inability of this model to give accurate enough results in various cases.

Thus, while momentum models continued to be applied for increasing number of problems and new areas other than aeronautic systems (see for example its application to wind energy problems in Ref. [4]), other researchers investigated the inaccuracies associated with this model. It started as early as 1925 ^[5] with Thoma who pointed out inconsistencies within the model. Goorjian ^[6] showed that when the differential form of the equation of axial momentum is combined with the other equations of the model, it leads to a contradiction. Rauh and Seelert ^[7] discussed problems with the model, associated with Betz theory of optimum efficiency of wind turbines. Van Kuik ^{[8],[9]} examined the singularity at the edge of an actuator disk and deduced the presence of a singular vortex carrying an edge force. He showed that allowance for this edge force may improve the accuracy of performance prediction of rotors. In a later paper ^[10] the author continued to discuss the inconsistencies associated with the classical actuator disk momentum theory. He ended up concluding that the origin of the inconsistency is not known yet, and thus it is not clear what changes are required in the modeling of the momentum balance in order to remove the inconsistencies. More recently Spalart ^[11] presented a mathematical model of the flow induced by an actuator disk in axial translation, which is more accurate than the classical solutions. While performance

results of rotor in hover were unchanged, common assumptions were proven to be incorrect, resulting in a different flow field through the rotor.

The above described inconsistencies associated with the classical momentum theory, lead various researchers to develop more accurate actuator disk models ^{[12]-[18]}. More recently Conway developed an analytical theory for a linearized actuator disk ^[19] and then extended it to a heavily loaded actuator disk with non-uniform loading ^[20]. The semi-analytical method takes the contraction of the slipstream into account. Although the above mentioned models may offer a better accuracy than the momentum models, since they are based on a solution of the flow equations in the entire flow field, these models are much more complicated and require long computations. Thus these models lose the main benefit of actuator disk models, namely their simplicity and efficiency.

The present paper presents a new actuator disk model, similar in its nature to the momentum model. This new model does not involve a solution of the entire flow field, but rather concentrate on the characteristics of the flow through the disk and in the far wake. The flow through the disk is modeled by a distribution of sinks which determine the axial and radial components of the induced flow. Only the integral form of conservation of axial momentum is applied, rather than its non-accurate differential form. The approximation of the present new model includes an assumption about the distribution of the pressure over the disk. Comparisons between the results of the present model and exact results of Conway ^[20] exhibit good agreement between both. Further comparisons with test results of a hovering rotor, show that the present new model exhibits a better agreement with the test results than the results of a general momentum model.

2 DESCRIPTION OF THE NEW MODEL

A rotary-wing system (rotor, propeller, wind turbine, etc.) in an incoming axial flow is considered. The system includes N_b identical blades. A cylindrical system of coordinates, (r, ψ, z) , will be used during the derivations. This is a non-rotating system that is attached to the hub center. The z axis coincides with the axis of rotation and points in the downstream direction, while r and ψ are the radial and angular (azimuthal) coordinates, respectively. It should be noted that ψ is positive in the counter-clockwise direction as seen by an upstream observer. The blades are rotating with an angular velocity Ω about the z axis. The incoming flow has a velocity V in the positive z direction (as seen by an observer on the rotor hub).

The blade root is located at $z=0$. Thus the plane $z=0$ is defined as the plane of rotation. Due to the action of the blades, velocities are induced over the entire space. The induced velocity at any point is in general a function of the time, t . Thus the resultant velocity at any point, at time t , $\mathbf{V}(r, \psi, z, t)$, equals:

$$\mathbf{V}(r, \psi, z, t) = v_r(r, \psi, z, t) \cdot \mathbf{e}_r + v_\psi(r, \psi, z, t) \cdot \mathbf{e}_\psi + [V + v_z(r, \psi, z, t)] \cdot \mathbf{e}_z \quad (1)$$

$\mathbf{e}_r, \mathbf{e}_\psi,$ and \mathbf{e}_z is a triad of unit vectors in the radial, circumferential, and axial directions, respectively. It should be noted that \mathbf{e}_r and \mathbf{e}_ψ are functions of ψ . $v_r(r, \psi, z, t)$, $v_\psi(r, \psi, z, t)$, and $v_z(r, \psi, z, t)$ are the radial, circumferential, and axial components of the induced velocity, respectively.

The pressure at any point is $[p_\infty + p(r, \psi, z, t)]$, where p_∞ is the pressure far from the disk.

The entire flow field is divided into three main regions:

- a) The actuator disk – The volume occupied by the rotating blades.
- b) The wake – Includes the fluid that has passed through the actuator disk.
- c) The rest of the flow field

In what follows, the three regions will be considered.

2.1 The actuator disk

It is assumed that the blades are slender and the distance between any material point of the blades and the plane of rotation is small compared to the radial coordinate of the same material point. Thus the thickness of the actuator disk will be neglected.

Each blade is represented by its quarter-chord line (see Figure 1), which is the line connecting the quarter chord points of all the cross-sections. The blade's cross-sections are normal to the quarter-chord line. In the case of straight blades, the quarter-chord line is a radial line. In the case of curved blades, the quarter-chord line is a curved line, lying in the plane of rotation.

Each point along the quarter-chord line is defined by its radial coordinate r . The radial coordinate of the blade tip, R , defines the radius of the actuator disk.

Consider now an annulus of the actuator disk (see Figure 1) which is defined by its radius r and width dr . The outer and inner radii of the annulus are $(r + dr/2)$ and $(r - dr/2)$, respectively. Inside this annulus, N_b blade elements are rotating. The length of each element is $dl(r)$, measured along the quarter-chord line, where:

$$dl(r) = \frac{dr}{\cos[\Lambda(r)]} \quad (2)$$

$\Lambda(r)$ is the local sweep angle, which is positive in the case of forward sweep (in Figure 1 the sweep angle is negative).

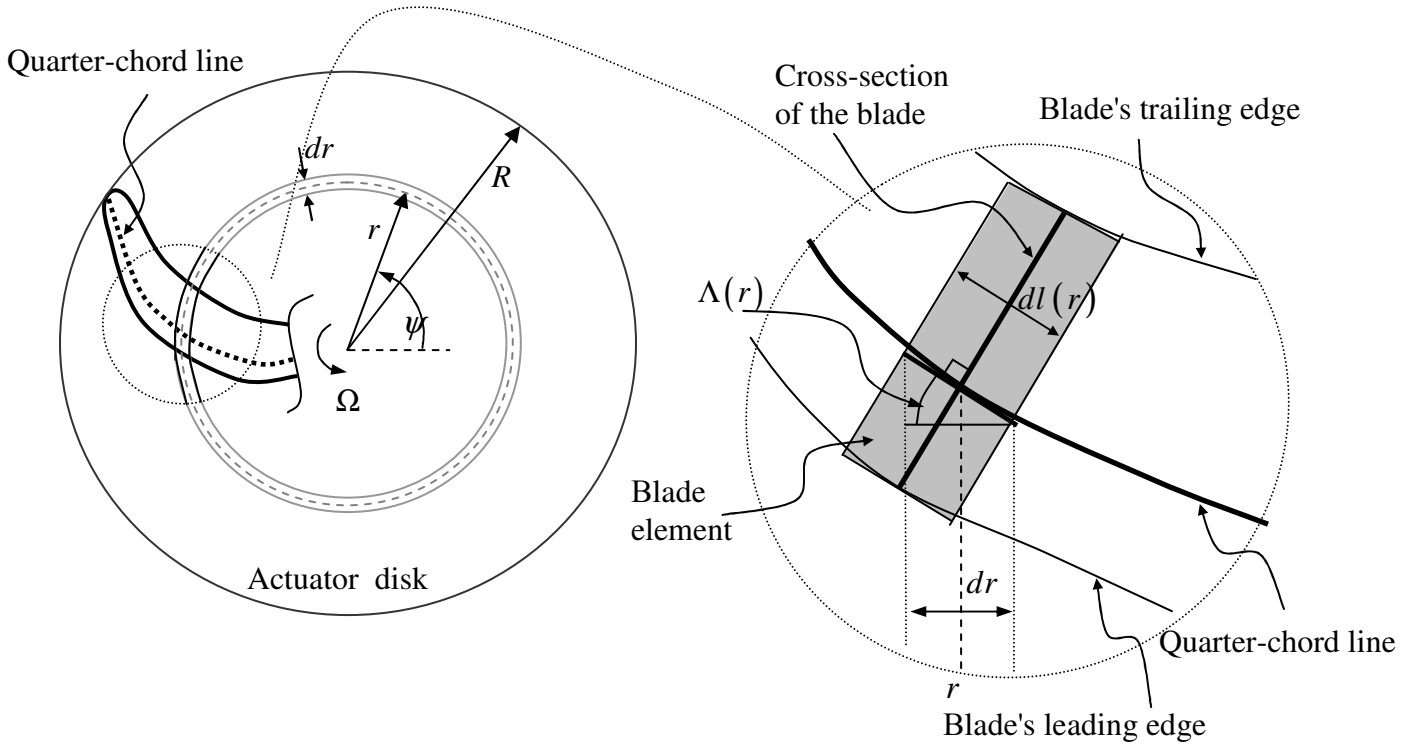


Figure 1: The actuator disk and a representative blade

The cross-section r has a chord length $c(r)$ and its pitch angle (the angle between the chord line and the plane of rotation) is $\theta(r)$ (see Figure 2). For a blade rotating at a constant angular speed Ω :

$$\psi(r) = \psi_0(r) + \Omega \cdot t \quad (3)$$

Where $\psi_0(r)$ is the angular location, of cross-section r , at $t=0$.

The flow field at cross-section r , which is located at azimuth ψ , is shown in Figure 2. $U(r, \psi)$ is the resultant velocity at the blade cross-section and is a function of the incoming flow velocity, V , blade rotation speed, Ω , sweep angle, $\Lambda(r)$, and the three components of the induced velocity “seen” by the cross-section r when located at an azimuth angle, ψ : $w_z(r, \psi)$, $w_\psi(r, \psi)$, and $w_r(r, \psi)$. The last terms are not functions of time since a “steady” case is considered.

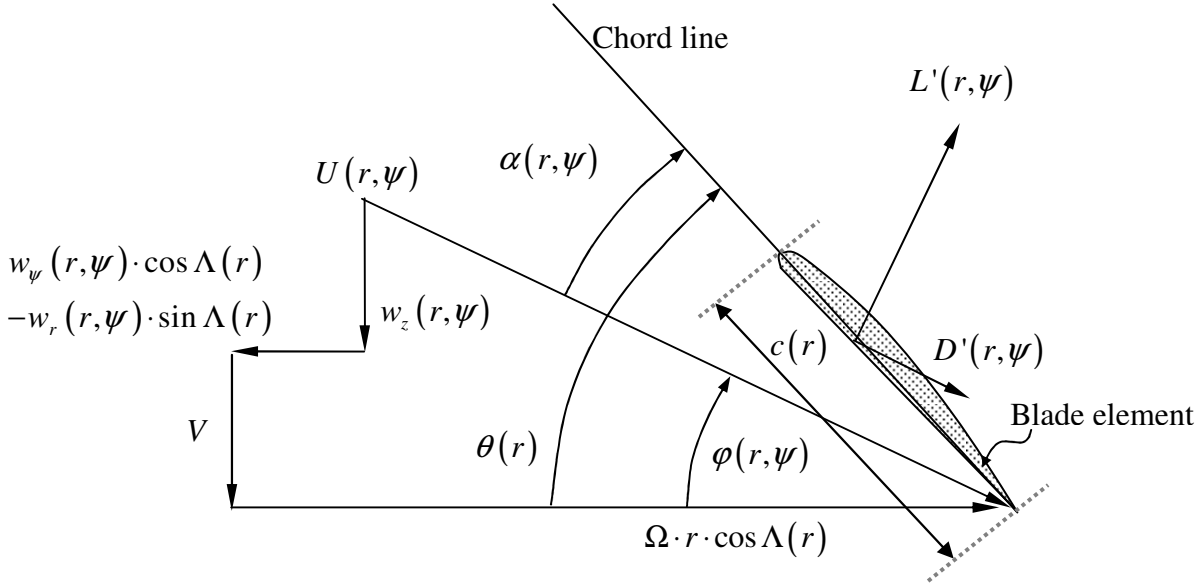


Figure 2: Cross-section of a blade-element

According to the usual blade-element approach, it is assumed that each cross-section, which is not at the close vicinity of the blade tip or root, behaves as the same cross-section in an identical two-dimensional flow. Thus the two components of the cross-sectional aerodynamic force per unit length, the lift (the component perpendicular to $U(r, \psi)$) and the drag (the component in the $U(r, \psi)$ direction), are respectively:

$$L'(r, \psi) = \frac{1}{2} \cdot \rho \cdot U^2(r, \psi) \cdot c(r) \cdot C_l[\alpha(r, \psi), M(r, \psi), \text{Re}(r, \psi)] \quad (4a)$$

$$D'(r, \psi) = \frac{1}{2} \cdot \rho \cdot U^2(r, \psi) \cdot c(r) \cdot C_d[\alpha(r, \psi), M(r, \psi), \text{Re}(r, \psi)] \quad (4b)$$

ρ is the fluid mass density. C_l and C_d are the cross-sectional lift and drag coefficients, respectively, which are functions of the cross-sectional angle of attack, $\alpha(r, \psi)$, Mach number, $M(r, \psi)$, and Reynolds number, $\text{Re}(r, \psi)$.

Near the blade tip or blade root, C_l and C_d should be corrected for three-dimensional effects. This correction can be obtained by multiplying the two-dimensional coefficients by correction factors.

$F_r'(r, \psi)$, $F_\psi'(r, \psi)$, and $F_z'(r, \psi)$ are the radial, circumferential and axial components, respectively, of the aerodynamic force that acts on a unit length of the blade, at cross-section r , which is located at an azimuth angle ψ . Based on the previous derivations, Figure 1, and Figure 2:

$$F_r'(r, \psi) = \{L'(r, \psi) \cdot \sin \varphi(r, \psi) + D'(r, \psi) \cdot \cos \varphi(r, \psi)\} \cdot \sin \Lambda(r) \quad (5a)$$

$$F_\psi'(r, \psi) = -\{L'(r, \psi) \cdot \sin \varphi(r, \psi) + D'(r, \psi) \cdot \cos \varphi(r, \psi)\} \cdot \cos \Lambda(r) \quad (5b)$$

$$F_z'(r, \psi) = -L'(r, \psi) \cdot \cos \varphi(r, \psi) + D'(r, \psi) \cdot \sin \varphi(r, \psi) \quad (5c)$$

$\varphi(r, \psi)$ is the local inflow angle, defined in Figure 2.

The lift per unit length, $L'(r, \psi)$, is a result of the pressure difference between both sides of the cross-section. The average pressure difference of cross-section r , at azimuth angle ψ , is $\Delta p(r, \psi)$. Thus:

$$L'(r, \psi) = \Delta p(r, \psi) \cdot c(r) \quad (6)$$

$[p_\infty + p_0(r, \psi)]$ is the pressure of the incoming flow as seen by cross-section r , at an azimuth angle ψ . The average pressure on the upper and lower surfaces of that cross-section are $p_u(r, \psi)$ and $p_l(r, \psi)$, respectively, where:

$$\Delta p(r, \psi) = p_l(r, \psi) - p_u(r, \psi) \quad (7a)$$

$$p_u(r, \psi) = p_\infty + p_0(r, \psi) + \Delta p_u(r, \psi) \quad (7b)$$

$$p_l(r, \psi) = p_\infty + p_0(r, \psi) + \Delta p_l(r, \psi) \quad (7c)$$

Equation (7a) can also be written as follows:

$$\Delta p_u(r, \psi) = -k(r, \psi) \cdot \Delta p(r, \psi) \quad (8a)$$

$$\Delta p_l(r, \psi) = [1 - k(r, \psi)] \cdot \Delta p(r, \psi) \quad (8b)$$

$k(r, \psi)$ is a function of: $\alpha(r, \psi)$, $M(r, \psi)$, and, $Re(r, \psi)$.

According to the linear theory of inviscid flow around a two dimensional thin cross-section, $k(r, \psi) = 0.5$ (see appendix A). The viscid actual value can be obtained from measurements of the pressure around a cross-section in a two-dimensional flow, at various: angle of attack, Mach number, and Reynolds number – see Appendix A.

In the present axisymmetric and steady case (axial flow and a pitch angle that does not change with ψ), all the cross-sectional variables do not vary with ψ and are functions of r only. Thus, in what follows, the variable ψ will be dropped from the above defined functions associated with cross-section r .

The actuator disk approach is based on a time averaging of any variable at any point (r, ψ) of the disk. The averaging with time in the present case is obtained by multiply the time dependent variables by $\left\{ N_b \cdot c(r) \cdot \cos \varphi(r) / [2 \cdot \pi \cdot r \cdot \cos \Lambda(r)] \right\}$.

Thus, based on equations (6)-(8), the pressure just before the flow enters the actuator disk $(z=0^-)$, $p(r, 0^-)$, and the pressure right after the flow crosses the disk $(z=0^+)$, $p(r, 0^+)$, are:

$$p(r, 0^-) = p_\infty + p_0(r) - k(r) \cdot L'(r) \cdot \frac{N_b \cdot \cos \varphi(r)}{2 \cdot \pi \cdot r \cdot \cos \Lambda(r)} \quad (9a)$$

$$p(r, 0^+) = p_\infty + p_0(r) + [1 - k(r)] \cdot L'(r) \cdot \frac{N_b \cdot \cos \varphi(r)}{2 \cdot \pi \cdot r \cdot \cos \Lambda(r)} \quad (9b)$$

$P_r(r, z)$, $P_\psi(r, z)$, and $P_z(r, z)$ are the average radial, circumferential, and axial components of the body force per unit volume, that act on the flow while it passes through the actuator disk. After neglecting viscid effects (namely, neglecting the influence of $D'(r)$), using equations (5a,c), and averaging with respect to time, these components become:

$$P_r(r, z) = -\frac{N_b \cdot L'(r) \cdot \sin \varphi(r) \cdot \tan \Lambda(r)}{2 \cdot \pi \cdot r} \cdot \delta(z) \quad (10a)$$

$$P_\psi(r, z) = \frac{N_b \cdot L'(r) \cdot \sin \varphi(r)}{2 \cdot \pi \cdot r} \cdot \delta(z) \quad (10b)$$

$$P_z(r, z) = \frac{N_b \cdot L'(r) \cdot \cos \varphi(r)}{2 \cdot \pi \cdot r \cdot \cos \Lambda(r)} \cdot \delta(z) \quad (10c)$$

$\delta(z)$ is the impulse Delta (Dirac Delta) function.

After the application of the averaging process, the components of the induced velocity and the pressure, for the present axisymmetric case, become functions of r and z only. At the disk, the induced velocity components are $w_r(r)$, $w_\psi(r)$, and $w_z(r)$.

The axisymmetric, inviscid, and incompressible momentum equations, of the flow through the actuator disk, are:

$$v_r \cdot \frac{\partial v_r}{\partial r} + (V + v_z) \cdot \frac{\partial v_r}{\partial z} - \frac{1}{r} \cdot v_\psi^2 = \frac{1}{\rho} \cdot \left(-\frac{\partial p}{\partial r} + P_r \right) \quad (11a)$$

$$v_r \cdot \frac{\partial v_\psi}{\partial r} + (V + v_z) \cdot \frac{\partial v_\psi}{\partial z} + \frac{1}{r} \cdot v_r \cdot v_\psi = \frac{1}{\rho} \cdot P_\psi \quad (11b)$$

$$v_r \cdot \frac{\partial v_z}{\partial r} + (V + v_z) \cdot \frac{\partial v_z}{\partial z} = \frac{1}{\rho} \cdot \left(-\frac{\partial p}{\partial z} + P_z \right) \quad (11c)$$

The continuity equation for this case is:

$$\frac{1}{r} \cdot \frac{\partial(r \cdot v_r)}{\partial r} + \frac{\partial v_z}{\partial z} = 0 \quad (12)$$

All the variables appearing in equations (11a,c) and (12) are functions of r and z .

Integration with respect to z , of the continuity equation (12), from $z=0^-$ to $z=0^+$, results in:

$$v_z(r, 0^+) - v_z(r, 0^-) = 0 \quad (13)$$

Equation (21) indicates that there is a continuity of the axial velocity through the disk, namely:

$$v_z(r, 0^+) = v_z(r, 0^-) = w_z(r) \quad (14)$$

Similar integration across the disk of equation (11c), using equation (14), indicates that:

$$p(r, 0^+) - p(r, 0^-) = \frac{N_b \cdot \cos \varphi(r) \cdot L'(r)}{2 \cdot \pi \cdot r \cdot \cos \Lambda(r)} \quad (15)$$

Equation (15) is in agreement with equations (9a,b).

Integration across the disk (with respect to z , from $z=0^-$ to $z=0^+$) of equations (11a,b) results in:

$$[V + w_z(r)] \cdot [v_r(r, 0^+) - v_r(r, 0^-)] = \frac{1}{\rho} \cdot \frac{N_b \cdot \sin \varphi(r) \cdot \tan \Lambda(r) \cdot L'(r)}{2 \cdot \pi \cdot r} \quad (16a)$$

$$[V + w_z(r)] \cdot [v_\psi(r, 0^+) - v_\psi(r, 0^-)] = \frac{1}{\rho} \cdot \frac{N_b \cdot \sin \varphi(r) \cdot L'(r)}{2 \cdot \pi \cdot r} \quad (16b)$$

Equation (16a) indicates that discontinuity in the radial component of the induced velocity occurs only in the case of curved blades or when $[V + w_z(r)] = 0$. On the other hand, only in the case of contra-rotating rotors (where the resultant term $[N_b \cdot \sin \varphi(r) \cdot L'(r)]$, of both rotors, becomes zero) or when $[V + w_z(r)] = 0$ and thus $\varphi(r) = 0$, there may be a continuity in the circumferential induced velocity. Based on conservation of angular momentum, assuming that a fluid particle does not cross the disk more than one time:

$$v_\psi(r, z) = 0 \quad \text{for} \quad z < 0 \quad (17)$$

It is also common to assume:

$$w_\psi(r) = \frac{1}{2} \cdot v_\psi(r, 0^+) \quad (18a)$$

$$w_r(r) = \frac{1}{2} \cdot [v_r(r, 0^+) + v_r(r, 0^-)] \quad (18b)$$

2.2 The wake

The wake starts at the actuator disk plane ($z = 0^+$) and continues to infinity ($z \rightarrow +\infty$). The lateral surface of the wake is defined by the streamlines that pass through the boundary of the actuator disk ($r = R$). As defined in the previous sub-section, at $z = 0^+$ the components of the induced velocity are: $v_r(r, 0^+)$, $v_\psi(r, 0^+)$, and $w_z(r)$. The pressure is $[p_\infty + p(r, 0^+)]$. In the previous sub-section an annulus of the disk was defined by its outer and inner radii, $(r + dr/2)$ and $(r - dr/2)$, respectively. The annulus width is dr . The streamlines that pass through the boundaries of the annulus define a control volume. The radius of this control volume at ($z \rightarrow +\infty$) is r' and its width is dr' , as shown in Figure 3.

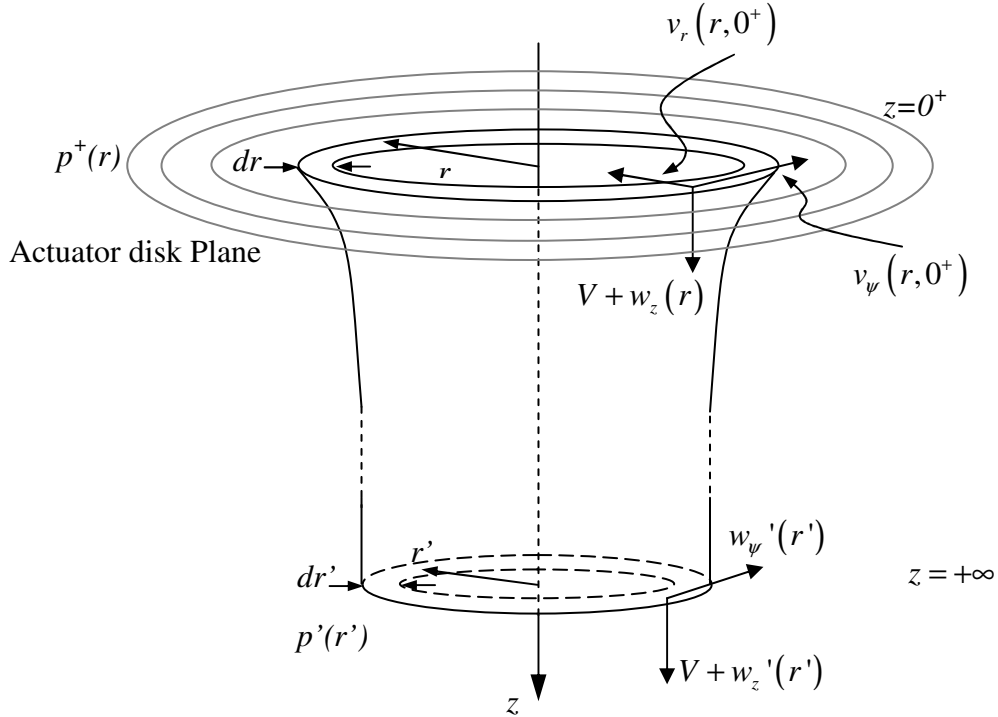


Figure 3: A control volume of the wake

r' is a function of r , thus:

$$r' = r'(r) \quad (19a)$$

$$dr' = dr'(r, dr) \quad (19b)$$

The induced velocity components at infinity are $w_r'(r)$, $w_\psi'(r)$, and $w_z'(r)$. According to the present assumptions $w_r'(r)$ becomes zero.

Due to conservation of mass:

$$[V + w_z(r)] \cdot r \cdot dr = [V + w_z'(r')] \cdot r' \cdot dr' \quad (20)$$

Bernoulli's equation along a streamline in the wake results in:

$$\begin{aligned} \frac{\rho}{2} \cdot \left\{ [V + w_z(r)]^2 + v_\psi^2(r, 0^+) + v_r^2(r, 0^+) \right\} + p(r, 0^+) = \\ = \frac{\rho}{2} \cdot \left\{ [V + w_z'(r')]^2 + w_\psi'^2(r') \right\} + p'(r') \end{aligned} \quad (21)$$

Equation (11a) implies:

$$\frac{dp'(r')}{dr'} = \rho \cdot \frac{w_\psi'^2(r')}{r'} \quad (22)$$

Where:

$$p'[r'(R)] = p_\infty \quad \text{for} \quad r' \geq r'(R) \quad (23)$$

Conservation of angular momentum and use of Equation (20) result in:

$$w_\psi'(r') \cdot r' = v_\psi(r, 0^+) \cdot r \quad (24)$$

All the equations of this sub-section are identical to the wake equations of the general momentum theory.

2.3 The rest of the flow field

Consider the half space $z < 0$. The actuator disk can be looked upon as an ‘‘apparatus’’ that sucks the fluid from that region and ‘‘pumps’’ it downstream into the wake. This mechanism can be modeled, for the region $z < 0$, as a distribution of sinks over the actuator disk. Since the present case is axisymmetric, the sink distribution should also be axisymmetric, namely a function of r only. The intensity of the sink distribution, per unit area of the disk, is denoted $\gamma(r)$.

In Appendix B, analysis of the flow field induced by such a sink distribution is presented. Based on Equations (14) and (B- 9):

$$\gamma(r) = 2 \cdot w_z(r) \quad (25)$$

Substitution of Equation (25) into Equation (B- 19) results in the following expression for the radial component of the induced velocity, right before the flow enters the disk:

$$v_r(r, 0^-) = \lim_{\varepsilon \rightarrow 0} \left\{ -\frac{1}{\pi} \cdot \int_{r'=0}^{r'=r-\varepsilon} w_z(r') \cdot r' \cdot [r \cdot A(r, z, r') - r' \cdot B(r, z, r')] \cdot dr' \right. \\ \left. - \frac{1}{\pi} \cdot \int_{r'=r+\varepsilon}^{r' \rightarrow \infty} w_z(r') \cdot r' \cdot [r \cdot A(r, z, r') - r' \cdot B(r, z, r')] \cdot dr' \right. \\ \left. + \frac{\gamma(r)}{2 \cdot \pi \cdot r} \cdot \varepsilon \cdot \ln \varepsilon \right\} \quad (26)$$

The various parameters that appear in Equation (26) are defined in Appendix B.

Since it is assumed that any fluid particle crosses the actuator disk only once, Bernoulli equation for a streamline that ends at a point $z = 0^-$ over the disk becomes (use is also made of Equation (17)):

$$\frac{1}{2} \cdot \rho \cdot [V \cdot w_z(r) + w_z^2(r) + v_r^2(r, 0^-)] + p(r, 0^-) = 0 \quad (27)$$

By using Equation (26) the value of $v_r(r, 0^-)$ is obtained also for points outside the disk area. Since for $r > R$ continuity of the flow and pressure across the plane $z=0$ should exist, it is clear that, in general, there is also an axial induced velocity outside the disk, $w_z(r > R)$. A first order approximation for $w_z(r)$ outside the disk area, is discussed in Appendix C.

2.4 The solution procedure

The present analysis includes an iterative solution procedure. Each iteration loop includes three stages:

- I) Finding the characteristics of the flow that passes through the actuator disk
- II) Finding the characteristics of the flow in the far wake
- III) Checking convergence and preparing the next iteration if necessary

There also may be an iterative procedure within each stage. In what follows the three stages will be described

2.4.1 Stage I

It is assumed that $p_0(r)$ is known. At the beginning of the first iteration. $p_0(r)$ can be chosen equal to zero.

There are eleven unknowns associated with this stage:

$$w_r(r), w_\psi(r), w_z(r), v_r(r, 0^-), v_r(r, 0^+), v_\psi(r, 0^+), p(r, 0^-), L'(r), \varphi(r), \alpha(r), U(r)$$

Based on the derivations of subsections 2.1 and 2.3, the following eight equations are used during the solution procedure of this stage: (4a), (9a), (16a,b), (18a,b), (26), (27).

There are additional three equations that are obtained from geometric relations presented in Figure 2:

$$\varphi(r) = \tan^{-1} \left[\frac{V + w_z(r)}{\Omega \cdot r \cdot \cos \Lambda(r) - w_\psi(r) \cdot \cos \Lambda(r) + w_r(r) \cdot \sin \Lambda(r)} \right] \quad (28a)$$

$$U(r) = \sqrt{[V + w_z(r)]^2 + [\Omega \cdot r \cdot \cos \Lambda(r) - w_\psi(r, \psi) \cdot \cos \Lambda(r) + w_r(r) \cdot \sin \Lambda(r)]^2} \quad (28b)$$

$$\alpha(r) = \theta(r) - \varphi(r) \quad (28c)$$

Thus the eleven equations are used to solve for the eleven unknowns. Because of the nonlinear nature of the equations, the solution procedure is iterative. The convergence is usually fast and stable.

It should be noted that the solution procedure includes an additional set of variables: $C_l(r), C_d(r), k(r)$. These variables are found based on the cross-sectional aerodynamic characteristics and flow conditions, namely: $\alpha(r), M(r), Re(r)$.

2.4.2 Stage II

The unknowns associated with this stage are: $p_r(r, 0^+), r'(r), w'_\psi(r), w'_z(r), p'(r)$.

The five equations that are solved in order to find these unknowns are: (15), (20), (21), (22), and (24). In addition the condition of Equation (23) is also applied.

2.4.3 Stage III

At this stage the convergence of the entire solution is checked. The convergence criterion is based on conservation of axial momentum. This condition is expressed by the following equation:

$$\int_0^R \Delta p(r) \cdot r \cdot dr - \int_0^{r'(R)} p'(r') \cdot r' \cdot dr' = \rho \cdot \int_0^{r'(R)} [V + w_z'(r')] \cdot w_z'(r') \cdot r' \cdot dr' \quad (29)$$

By using Equation (20), the last equation can be written as:

$$\int_0^R \Delta p_e(r) \cdot r \cdot dr = \rho \cdot \int_0^{r'(R)} [V + w_z'(r')] \cdot w_z'(r') \cdot r' \cdot dr' \quad (30a)$$

$$\Delta p_e(r) = \Delta p(r) - p'[r'(r)] \cdot \frac{V + w_z(r)}{V + w_z'[r'(r)]} \quad (30b)$$

$\Delta p_e(r)$ can be looked upon as an “equivalent” pressure difference across the disk. Thus, based on Equations (7b) and (8a), in order to satisfy the momentum equation, $p_0(r)$ is chosen as:

$$p_0(r) = k(r) \cdot p'[r'(r)] \cdot \frac{V + w_z(r)}{V + w_z'[r'(r)]} \quad (31)$$

The above described step (defining $p_0(r)$ by Equation (31)) still does not assure the conservation of axial momentum. Thus, if necessary, $k(r)$ will be varied by a certain constant factor, until Equation (28) is satisfied (based on a predetermined convergence criterion). If this factor is given by $(1+C)$, it simply indicates that Equation (31) should be replaced by the following one:

$$p_0(r) = (1+C) \cdot k(r) \cdot p'[r'(r)] \cdot \frac{V + w_z(r)}{V + w_z'[r'(r)]} - C \cdot k(r) \cdot \Delta p(r) \quad (32)$$

At this stage the value of $p_0(r)$ according to (32) is compared with the value of $p_0(r)$ that was used as an input to the first stage. If the difference between both is larger than a predetermined convergence criterion, a new iteration cycle is started.

It should be pointed out that the present iterative procedure is very stable and usually converges very rapidly, unlike the convergence procedure of the general momentum theory which in various cases suffers from numerical problems.

3 RESULTS

The new actuator disk model will be validated by comparing its results with theoretical results of Conway^[20] and test results that were reported by Landgrebe^[21].

3.1 Comparison with the results of Conway

Conway^[20] presented exact results for the flow field of an actuator disk. In his report Conway used the following definitions for the rotor advance ratio, J :

$$J = \frac{\pi \cdot V}{\Omega \cdot R} \quad (33)$$

and the thrust coefficient, C_{Th} :

$$C_{Th} = \frac{T}{\frac{1}{2} \cdot \rho \cdot R^2 \cdot V^2} \quad (34a)$$

$$(34b)$$

Where T is the total thrust and P is the required power.

Conway analysed three different disk loadings, $\Delta p(r)$ (see Figure 4):

- i) The disk loading has maximum at the disk center ($r=0$) and then decreases monotonically toward the disk rim, where its value becomes zero. There is no slipstream rotation [$v_\psi(r, z) = 0$] and $C_{Th} = 3.147$.
- ii) A typical rotor loading (increased loading at the outer part of the disk) with zero slipstream rotation. $C_{Th} = 0.9533$.
- iii) A typical rotor loading with slipstream rotation. $C_{Th} = 0.8903$ and $J = 1$.

In all three cases the loading distribution was obtained from the figures of Ref. [20] and thus certain inaccuracies may exist.

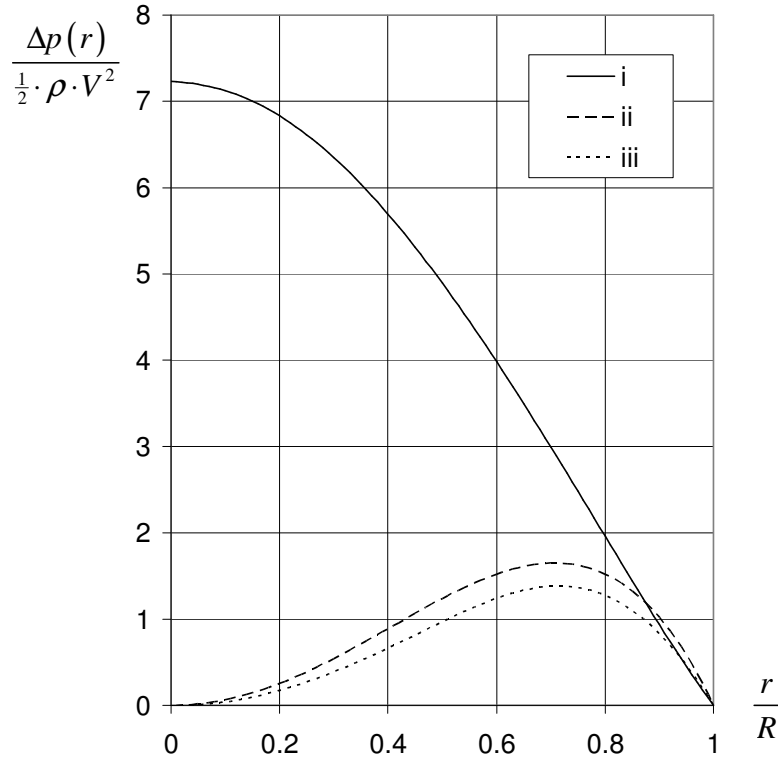


Figure 4: Conway's loads distributions

3.1.1 Case i

The iterative numerical procedure converges relatively fast. The value of C at convergence is $C=-0.07$. It shows that a relatively small $p_0(r)$ is required in order to satisfy the conservation of axial momentum.

The axial induced velocity through the disk, $w_z(r)$, is shown in Figure 5. There is a good agreement between the results of both models. A difference of $\sim 5\%$ in $w_z(r)$ exists at $r=0$, where this component obtains its maximum value. Good agreement is also shown for the negative axial induced velocity near the disk rim. The present approximation for the axial induced velocity outside the disk also seems to be satisfactory when taking into account the fact that the influence of this velocity on the flow through the disk is relatively small.

The radial induced velocity is shown in Figure 6. The agreement between the results of the two models is good with differences not exceeding 9%.

Figure 7 presents the axial induced velocity in the wake. While Conway gives results for $z=R$, the results of the present model are for the case $z \rightarrow \infty$. It can be seen that the wake at $z=R$ is almost fully developed.

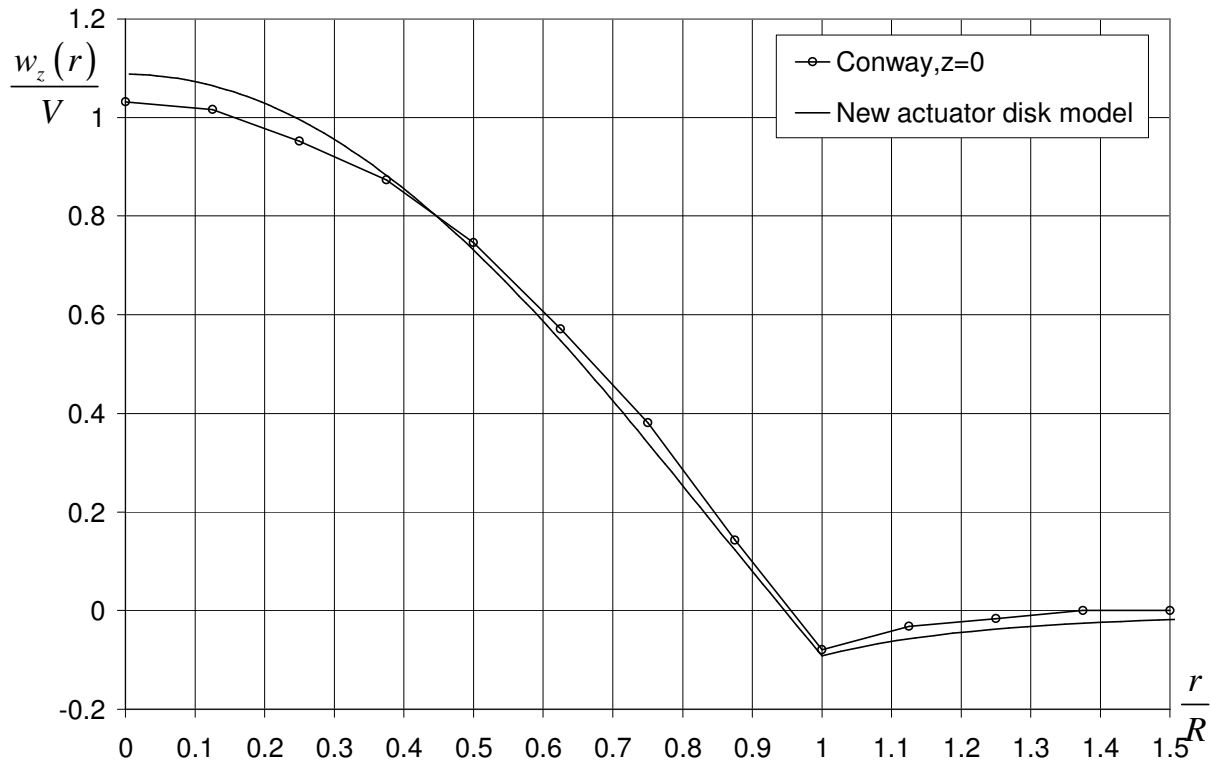


Figure 5: Conway's case i - Axial induced velocity at the disk plane

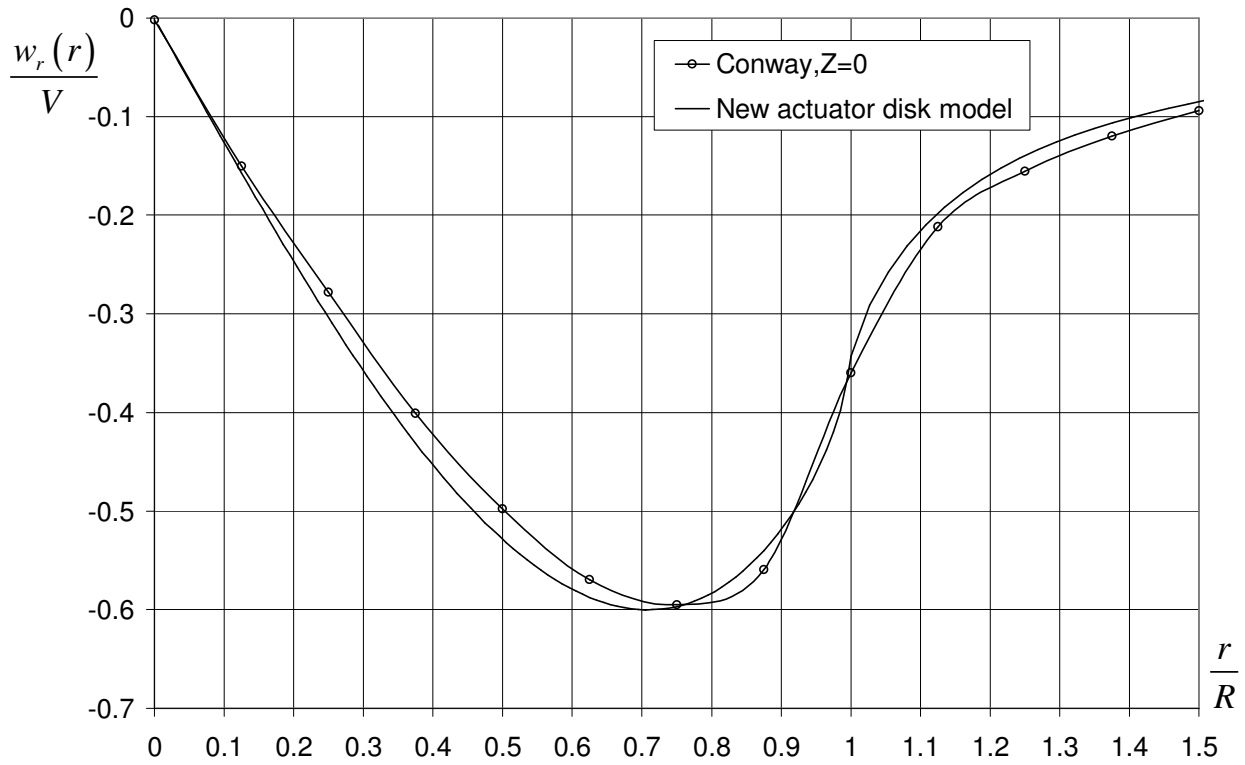


Figure 6: Radial Conway's case i - Radial induced velocity at the disk plane

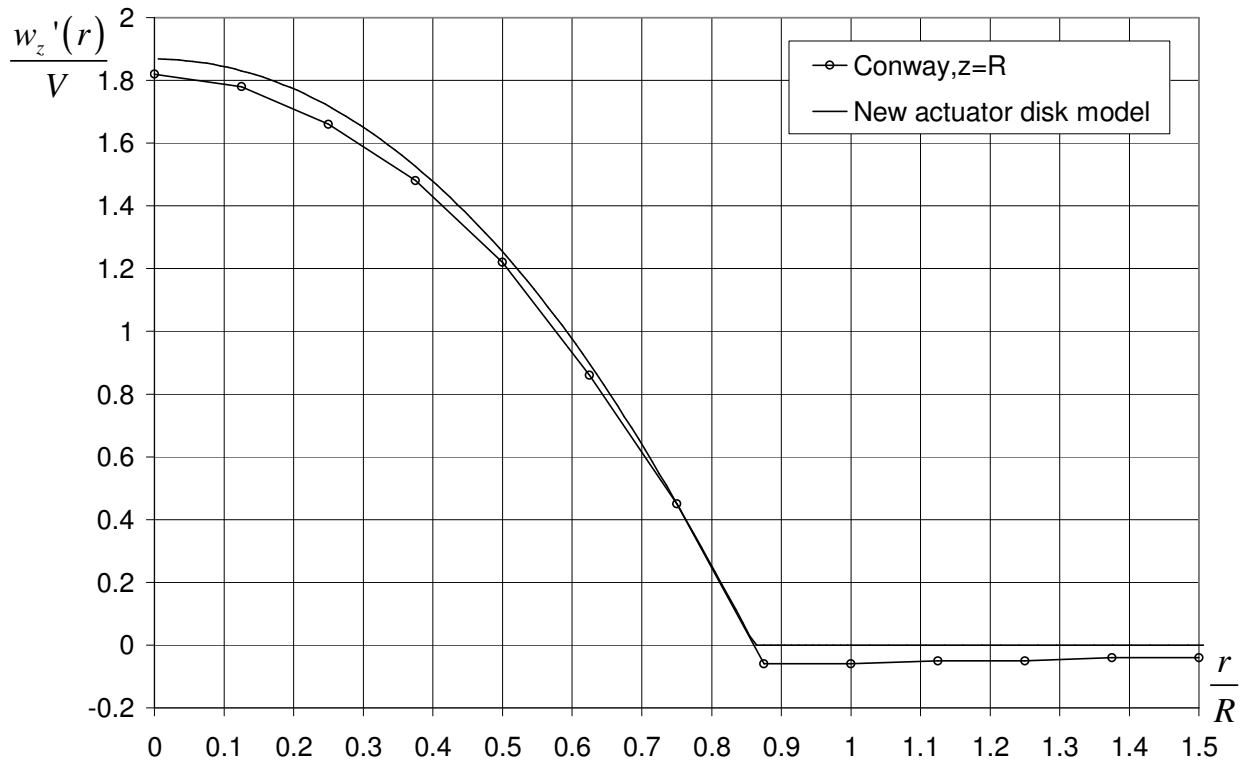


Figure 7: Conway's case i - Axial induced velocity in the far wake

3.1.2 Case ii

The convergence in this case is again stable and fast with $C=-0.04$. The axial induced velocity through the disk is shown in Figure 8. There is a fairly good agreement between the results of the two models. The differences at the maximum value reach a value of $\sim 5\%$. It should be noted that the negative induced velocity near the rim of the disk and for $r>R$ exhibits, again, a good agreement between the two models. On the other hand, Conway predicts a small negative induced axial velocity at the middle of the disk, while the present model practically predicts a zero axial induced velocity there.

The agreement between the radial component of the induced velocity, obtained by the two models, is good as shown in Figure 9.

The axial induced velocity in the wake is shown in Figure 10. As indicated for case i, the results of Conway are for $z=R$, while in the case of the present model the results are for $z \rightarrow \infty$. Again, it can be seen that the flow at $z=R$ is almost fully developed. The value of the negative induced velocity at $r=R$ is fairly large. Examination of Figure 15 of Ref. [20], indicates that this value approaches zero as z is increased.

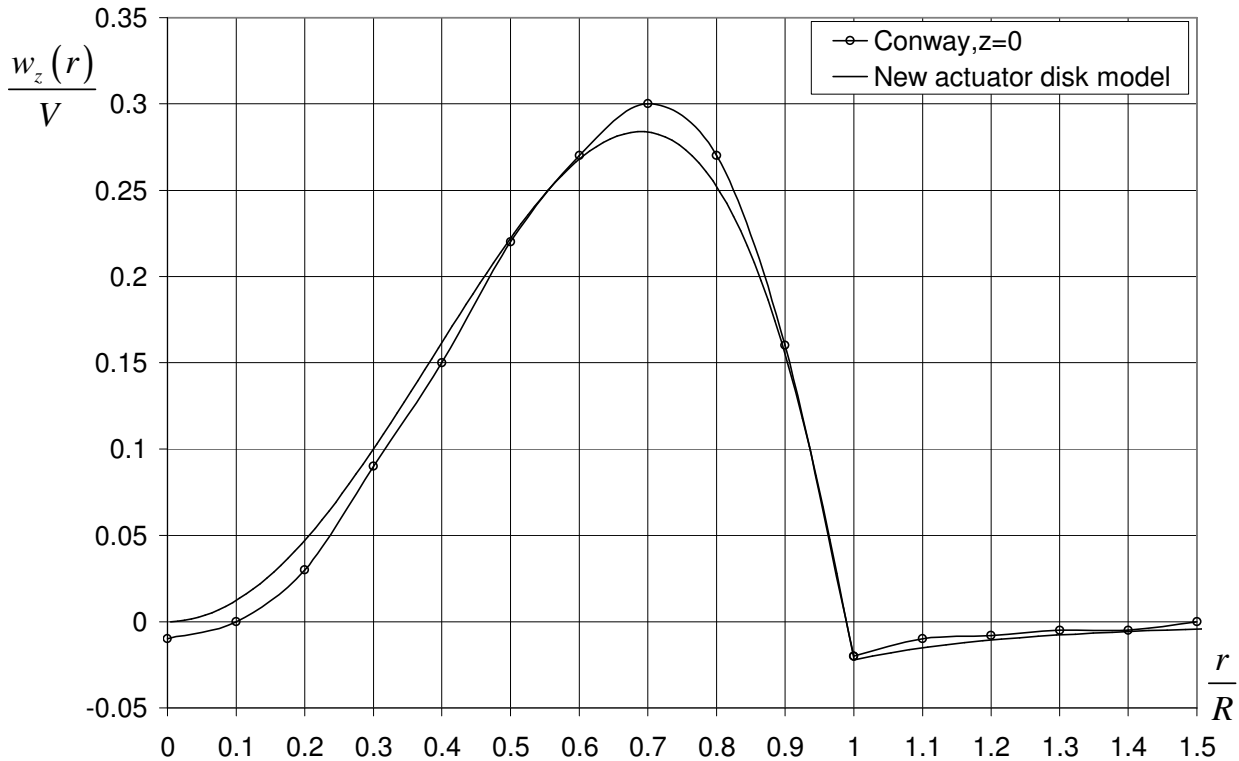


Figure 8: Conway's case ii - Axial induced velocity at the disk plane

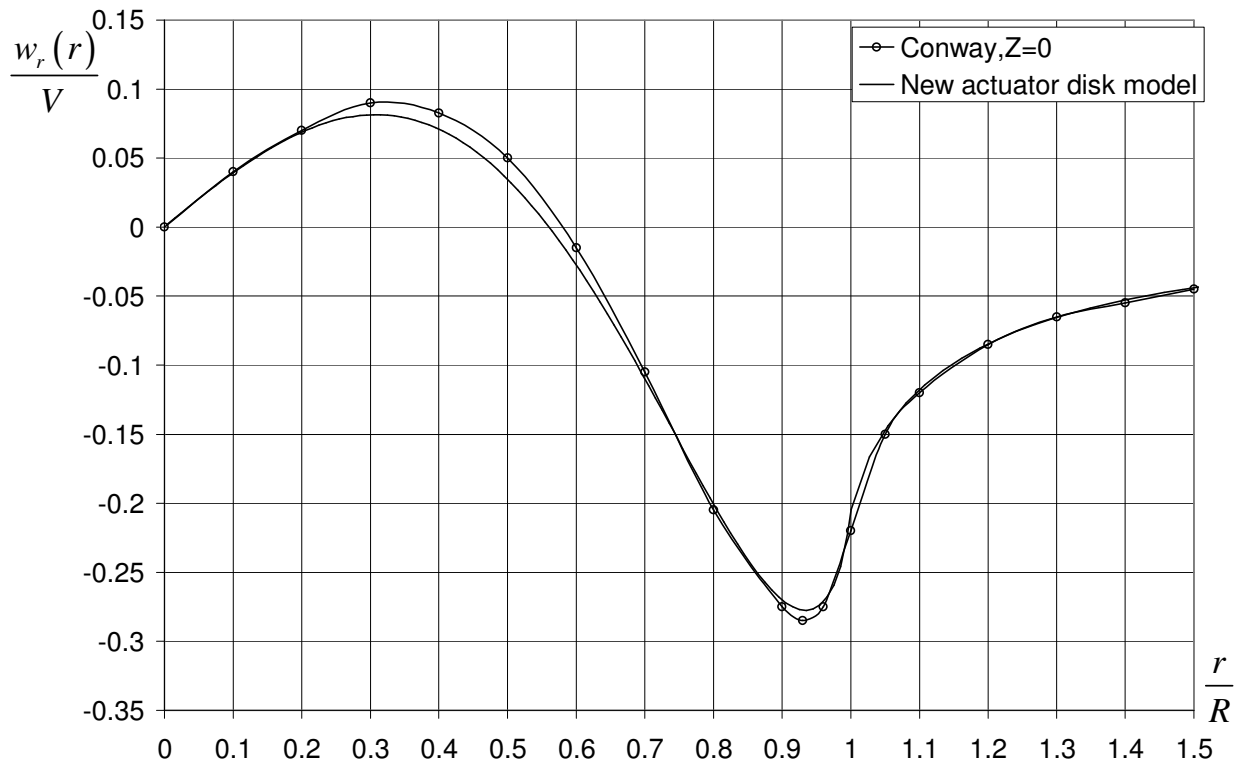


Figure 9: Radial Conway's case ii - Radial induced velocity at the disk plane

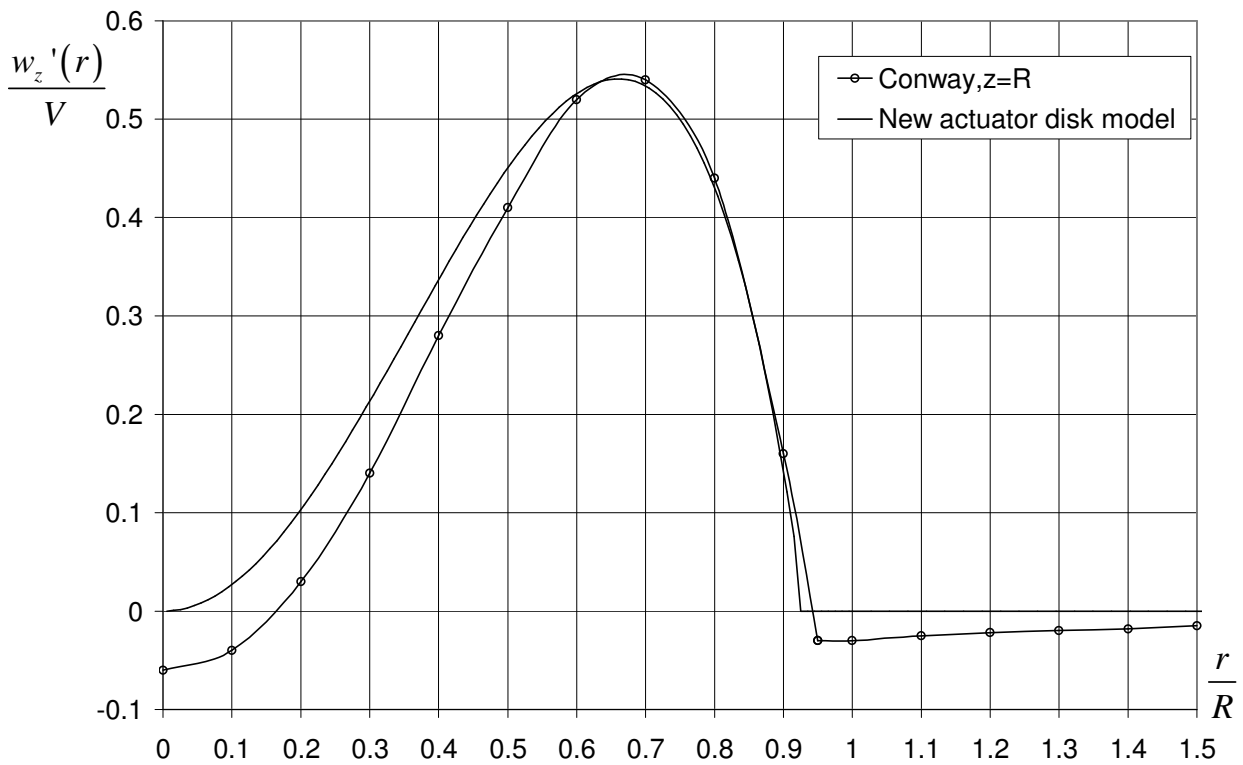


Figure 10: Axial Conway's case ii - Axial induced velocity in the far wake

3.1.3 Case iii

The convergence parameter in this case is $C=-0.04$. It shows again that the magnitude of $p_0(r)$ required for obtaining conservation of axial momentum is relatively small.

The agreement between the axial induced velocity as obtained from both models is excellent, as shown in Figure 11. It should be noted again that there is a good agreement of the negative values near the disk rim and for $r>R$.

There is also an excellent agreement between the radial and tangential components of the induced velocities through the disk – $w_r(r)$ and $w_\psi(r)$, respectively – as shown in Figure 12 and Figure 13.

Figure 14 and Figure 15 show also excellent agreement between both models concerning the axial and tangential components in the far wake ($z \rightarrow \infty$). The results indicate that the radii of the far wake, according to both models, namely $r'(R)$, practically obtain identical values.

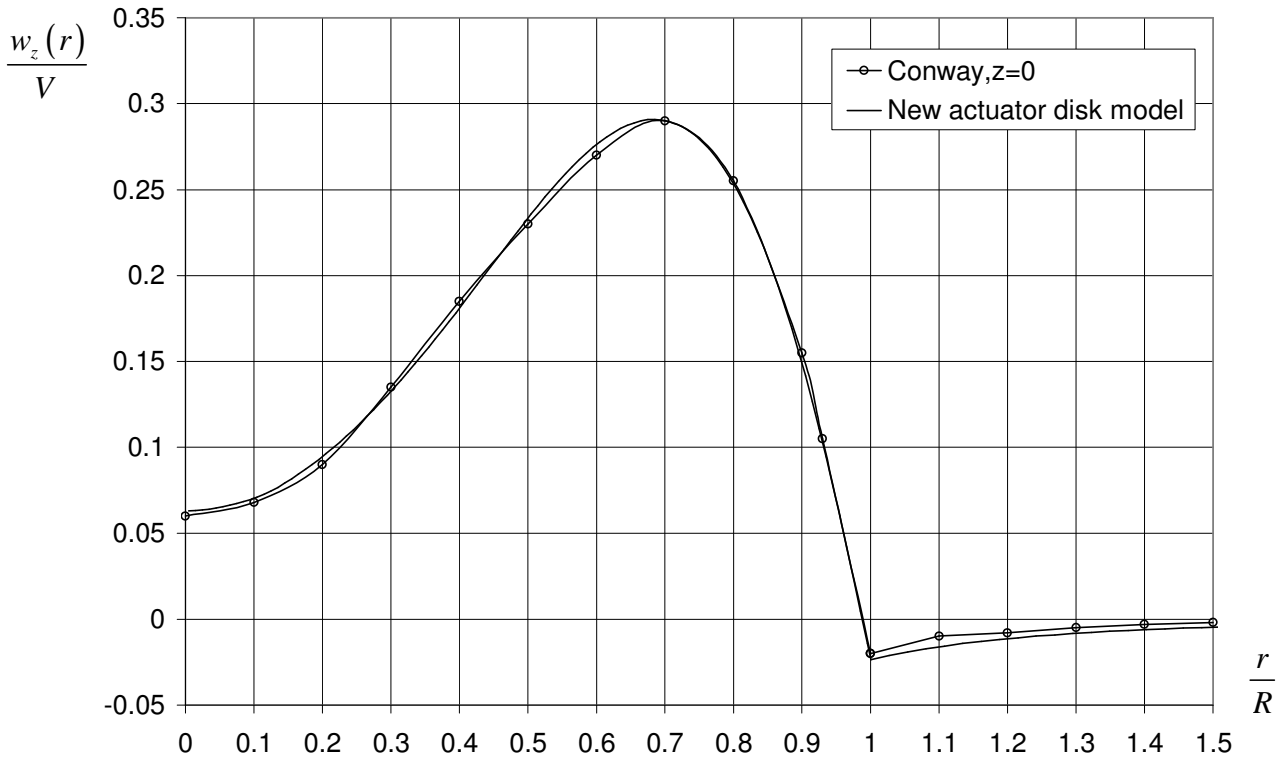


Figure 11: Conway's case iii - Axial induced velocity at the disk plane

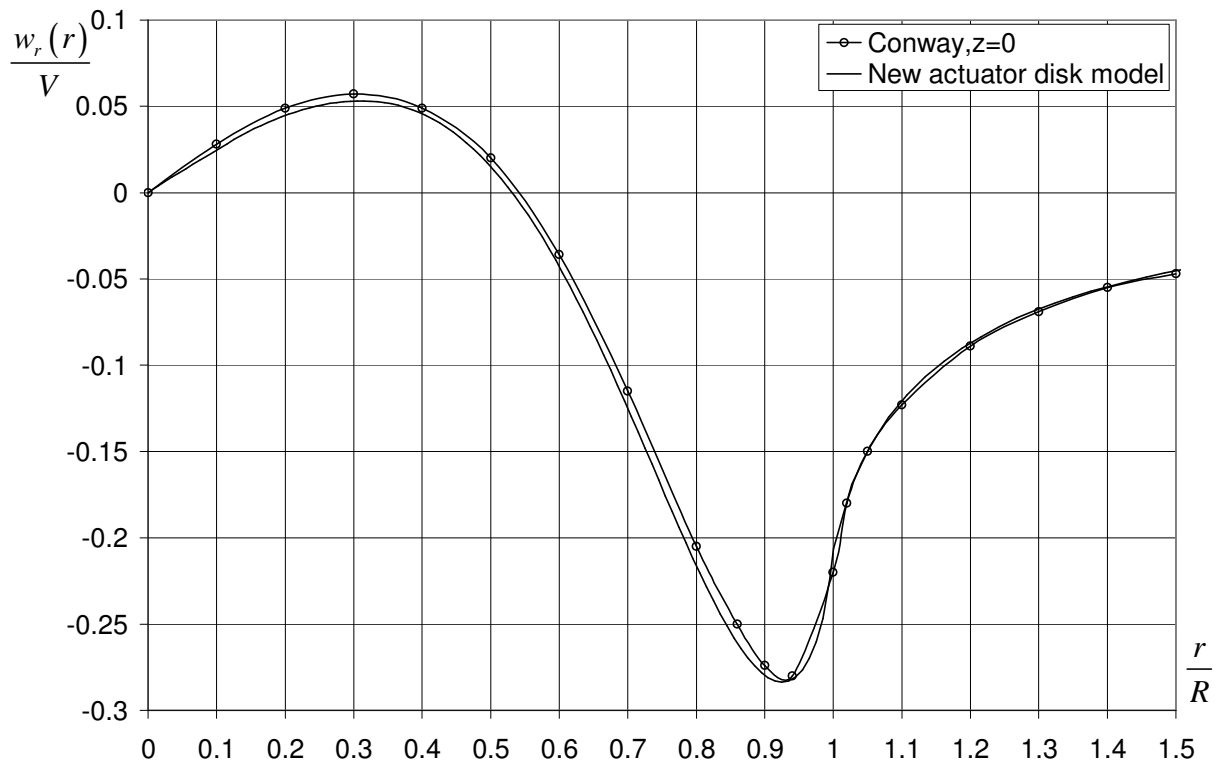


Figure 12: Conway's case iii - Radial induced velocity at the disk plane

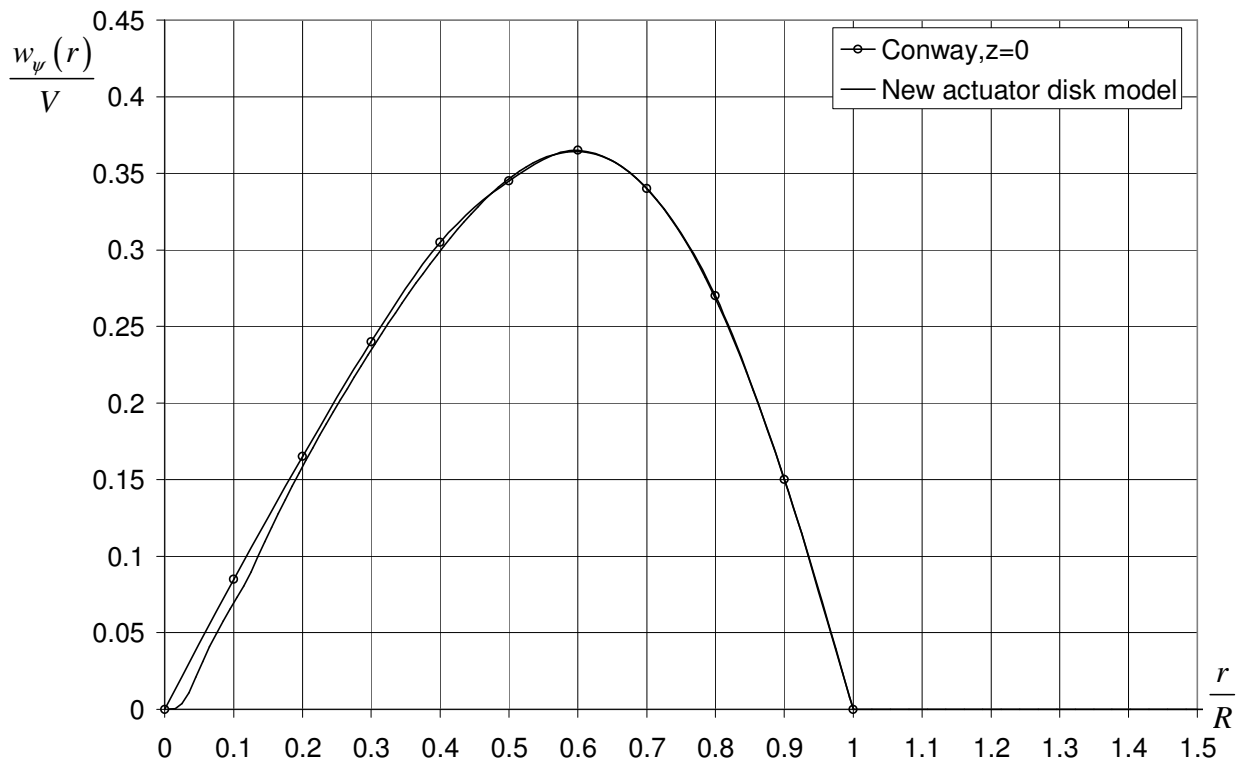


Figure 13: Conway's case iii - Circumferential induced velocity at the disk plane

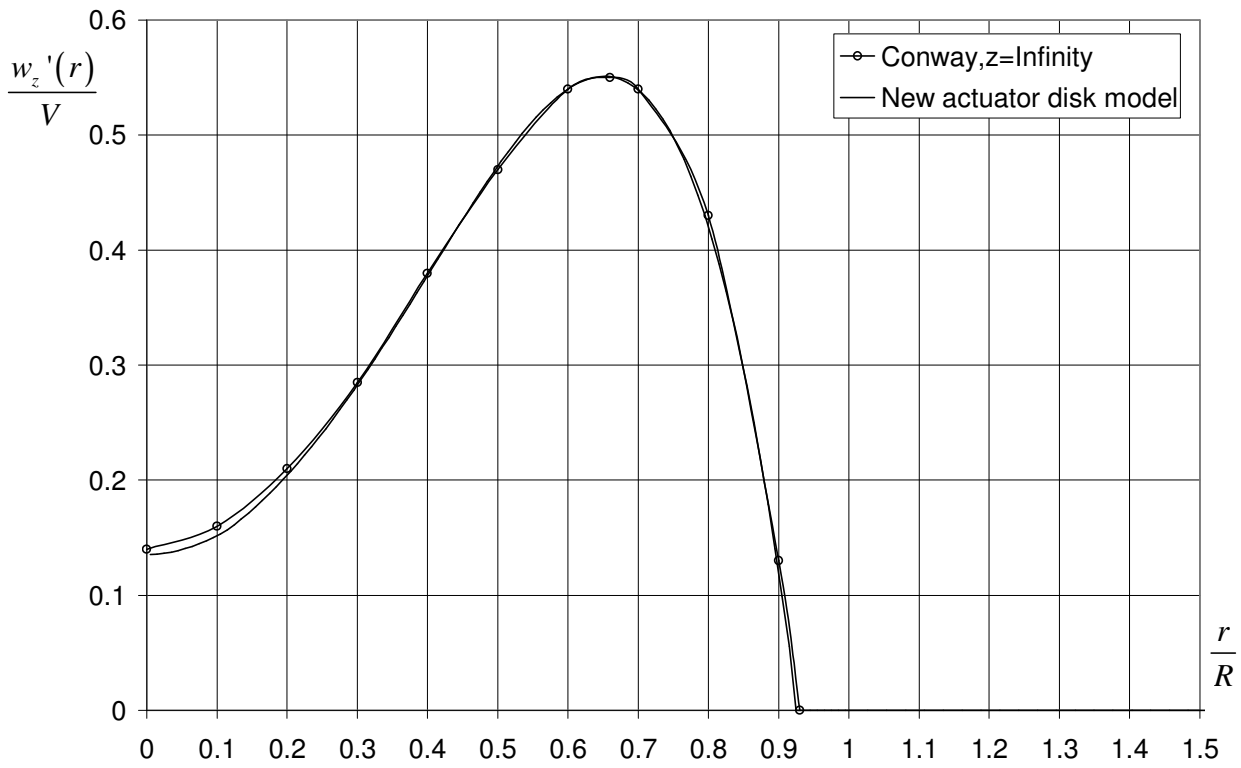


Figure 14: Conway's case iii - Axial induced velocity in the far wake

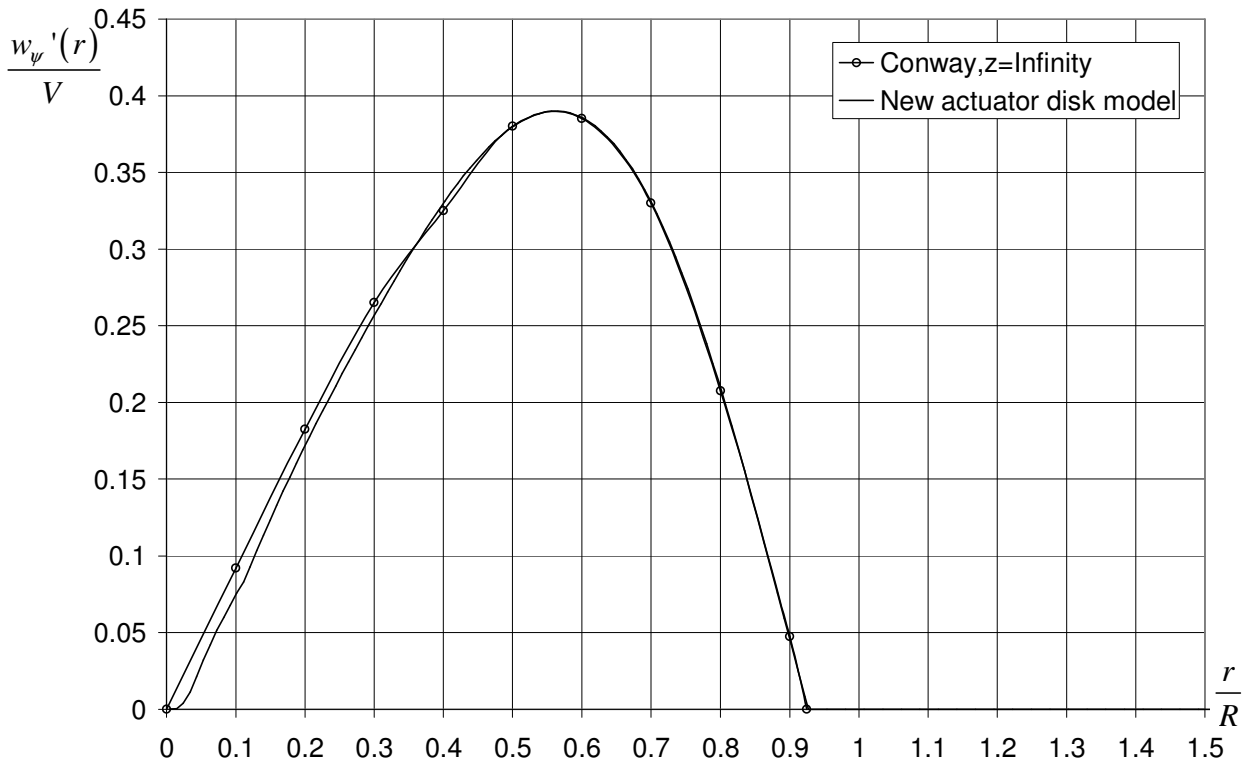


Figure 15: Conway's case iii - Circumferential induced velocity in the far wake

3.2 Comparison with the test results of Landgrebe

Landgrebe^[21] presented test results for various rotor models at hover. The models differ by: number of blades, N_b , built-in pre-twist of the blades, θ_{tw} , the pitch angle of the blade given at $r=0.75R$, $\theta_{0.75}$, and the blade chord, c . The detailed geometry of the blades is given in Ref. [21].

Only results for untwisted blades are presented here. Those blades have a radius $R=0.679[m]$ and constant chord $c=0.0373[m]$. The blade cross-section is NACA 0012. The tests were conducted at constant rotation speed of $3000[RPM]$.

The results include the thrust coefficient, C_T , and the power coefficient, C_p , which are defined below:

$$C_T = \frac{T}{\rho \cdot \pi \cdot R^2 \cdot (\Omega \cdot R)^2} \quad (35a)$$

$$C_p = \frac{P}{\rho \cdot \pi \cdot R^2 \cdot (\Omega \cdot R)^3} \quad (35b)$$

T is the rotor thrust while P is the required power.

The thrust coefficient, C_T is shown in Figure 16, for various number of blades ($N_b = 2, 4, 6, 8$), as a function of the blade pitch angle, $\theta_{0.75}$. The agreement between the results of the present model and test results is good, except for large number of blades ($N_b = 6, 8$) at small pitch angles ($\theta_{0.75} = 6[\text{deg}]$). The results of the general momentum model give higher values of thrust coefficients that exhibit difference of up to 20%.

The power coefficient, C_p , is shown in Figure 17. Except for large pitch angles, there is a fairly good agreement between the results of the present model and the general momentum model, and both exhibit good agreement with the test results. At larger pitch angles ($\theta_{0.75} > 10[\text{deg}]$), while the present model still exhibits good agreement with the test results, the results of the general momentum model are lower than the results of the present model and exhibit increasing deviations from the test results.

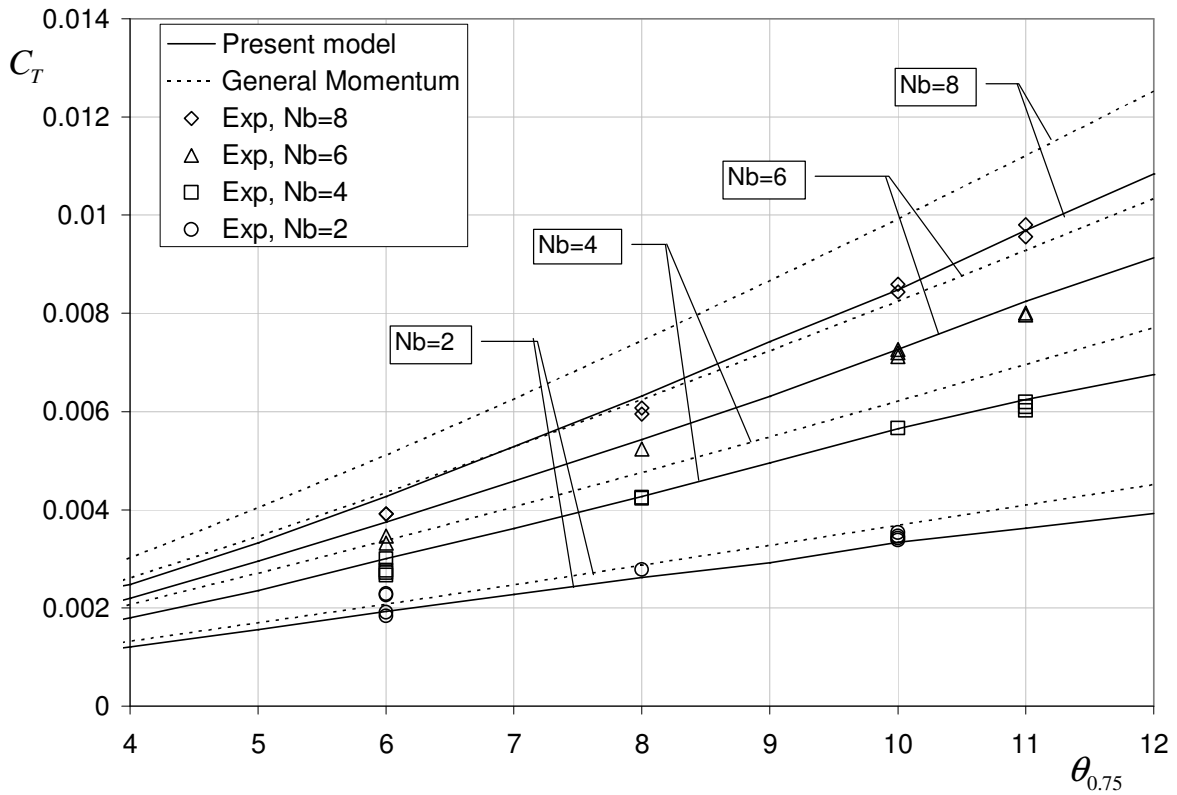


Figure 16: Comparison with Landgrebe's ^[21] results - thrust coefficient

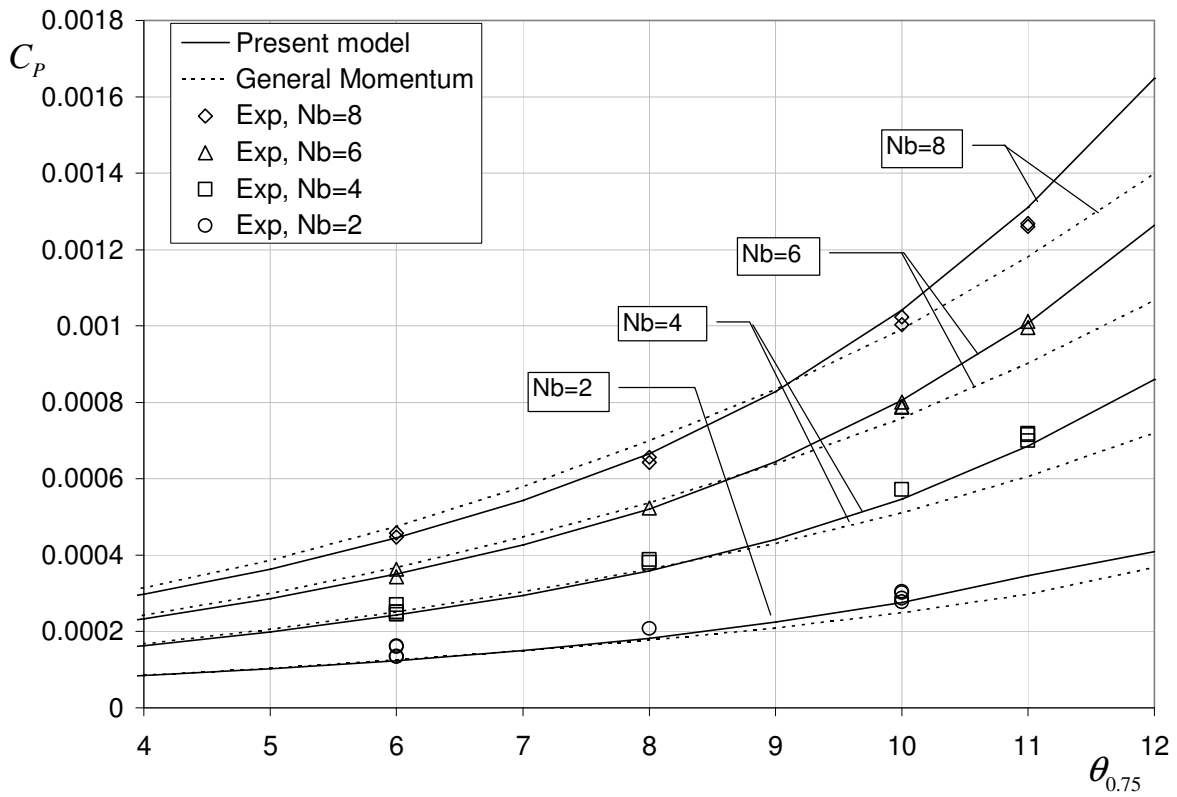


Figure 17: Comparison with Landgrebe's ^[21] results - power coefficient

4 CONCLUSIONS

A new actuator disk model has been presented. The derivation of the model for the case of an axial, axisymmetric flow through the disk was discussed.

The entire flow field is divided into three different regions that include: the actuator disk, the wake, and the rest of the flow field. The actuator disk is analyzed by using a common blade-element approach. Swept blades can be dealt with, as well as straight blades. It is assumed that the pressure difference on both sides of the disk is a result of time averaging, at any point of the disk, of the pressure difference between both sides of the blade-elements that pass through that point. The pressure on both sides of the airfoil is obtained from either theoretical derivations, or from test results of a two dimensional flow over the same airfoil. This data is in general a function of: the angle of attack, Mach number and Reynolds number. The relations between the flow characteristics before the flow crosses the disk and right after it passes it, are obtained by examining the appropriate momentum and continuity equations.

The equations associated with the wake are identical to the wake equations that are used in the general momentum theory. The analysis of the rest of the flow field includes the calculation of the induced velocities just before the flow crosses the disk. In order to calculate those induced velocities the influence of the disk on the flow is modeled by an axisymmetric distribution of sinks. It is shown that the intensity of the sinks, per unit area of the disk, is directly related to the magnitude of the axial induced velocity at that point. Integral relation yields the value of the radial component of the induced velocity at any point of the disk. The calculation of this integral involves singularity problems, which are treated by analytical derivations near the singular points. A first order approximation is used for calculating the axial induced velocities at the disk plane, at radial distances which are larger than the disk radius.

The solution of the highly nonlinear equations involves an iterative procedure. Usually this procedure is stable and converges relatively fast. The convergence criterion of the entire iterative procedure is based on conservation of the integral axial momentum.

Comparison of the results of the present model with those of the exact model of Conway shows a very good agreement. It should be noted that Conway's model is much more complicated and requires much longer computing time. It is also important to note that negative value of the induced velocity near the rim of the actuator disk agrees very well with the upwash obtained by Conway. The general momentum theory is not capable of predicting this upwash. There is also a very good agreement between the radial induced velocity as calculated by Conway, and the present results, indicating that the modeling of the disk as a distribution of sinks is a probably a correct representation.

Comparison of the results of the present model with the test results of Landgrebe shows a fair agreement, while the general momentum results exhibit increasing differences.

The present results are promising and indicate that the new model should be further validated against existing theoretical results of more detailed and more accurate actuator disk models' or further validated against additional test results. Moreover, it seems that the present model can be extended to include cases of incoming inclined flow (relative to the disk) which describes a helicopter rotor in forward flight.

APPENDIX A. THE AVERAGE PRESSURE RATIO, $k(r)$

The parameter $k(r)$ is defined by Equations (8a,b). $k(r)$ gives the ratio between the contribution of the upper and the lower surfaces of an airfoil, to the pressure difference between those two surfaces.

Consider a two-dimensional flow about an airfoil. The pressure of the undisturbed flow is p_∞ . x is a coordinate along the chord, where $x=0$ at the leading edge and $x=c$ at the trailing edge. The pressure at the upper surface is $[p_\infty + \Delta p_u(x/c)]$, while the pressure on the lower surface is $[p_\infty + \Delta p_l(x/c)]$.

The lift per unit length of the airfoil is L' and it is the result of a contribution of the upper surface, $\Delta L'_u$, and lower surface, $\Delta L'_l$, thus:

$$L' = \Delta L'_u + \Delta L'_l \quad (\text{A- 1})$$

The terms in Equation (A- 1) can be written as functions of the upper and lower pressures:

$$\Delta L'_u = - \int_0^1 \left[\Delta p_u \left(\frac{x}{c} \right) - \Delta p_{u0} \left(\frac{x}{c} \right) \right] \cdot d \left(\frac{x}{c} \right) \quad (\text{A- 2a})$$

$$\Delta L'_l = \int_0^1 \left[\Delta p_l \left(\frac{x}{c} \right) - \Delta p_{l0} \left(\frac{x}{c} \right) \right] \cdot d \left(\frac{x}{c} \right) \quad (\text{A- 2b})$$

$\Delta p_{u0}(x/c)$ and $\Delta p_{l0}(x/c)$ are the values of $\Delta p_u(x/c)$ and $\Delta p_l(x/c)$, respectively, for zero lift.

According to equations (8a,b), k is defined as follows:

$$\Delta L'_u = k \cdot L' \quad (\text{A- 3a})$$

$$\Delta L'_l = (1-k) \cdot L' \quad (\text{A- 3b})$$

Thus:

$$k = \frac{\Delta L'_u}{L'} = 1 - \frac{\Delta L'_l}{L'} \quad (\text{A- 4})$$

k is a function of the flow conditions, namely: the section angle of attack, α , free stream mach number, M , and Reynolds number, Re .

It is convenient to replace the pressure by the pressure coefficient, namely:

$$C_{Pu} \left(\frac{x}{c} \right) = \frac{\Delta p_u \left(\frac{x}{c} \right)}{\frac{1}{2} \cdot \rho \cdot u_0^2} \quad (\text{A- 5a})$$

$$C_{Pl} \left(\frac{x}{c} \right) = \frac{\Delta p_l \left(\frac{x}{c} \right)}{\frac{1}{2} \cdot \rho \cdot u_0^2} \quad (\text{A- 5b})$$

Where ρ is the fluid mass density and u_0 is the free stream velocity.

In the same manner $C_{Pu0}(x/c)$ and $C_{Pl0}(x/c)$ are defined based on $\Delta p_{u0}(x/c)$ and $\Delta p_{l0}(x/c)$, respectively.

Substitution of Equations (A- 5a,b) into Equations (A- 2a,b) and then into Equation (A- 4), result in:

$$k = \frac{-\int_0^1 \left[C_{Pu} \left(\frac{x}{c} \right) - C_{Pu0} \left(\frac{x}{c} \right) \right] \cdot d \left(\frac{x}{c} \right)}{\int_0^1 \left[C_{Pl} \left(\frac{x}{c} \right) - C_{Pu} \left(\frac{x}{c} \right) \right] \cdot d \left(\frac{x}{c} \right)} \quad (\text{A- 6})$$

For the simple case of an incompressible, ideal, two dimensional flow over a flat plate, the pressure coefficients are ^[22]:

$$C_{Pu}(\xi) = -2 \cdot \alpha \cdot \tan \frac{\xi}{2} \quad (\text{A- 7a})$$

$$C_{Pl}(\xi) = 2 \cdot \alpha \cdot \tan \frac{\xi}{2} \quad (\text{A- 7b})$$

$$C_{Pu0}(\xi) = 0 \quad (\text{A- 7c})$$

$$C_{Pl0}(\xi) = 0 \quad (\text{A- 7d})$$

Where ξ :

$$\frac{x}{c} = \frac{1 + \cos \xi}{2} \quad 0 < \xi < \pi \quad (\text{A- 8})$$

Substituting Equations (A- 7a,d) into Equation (A- 6), results in $k=0.5$.

In Figure (A- 1) the experimental value of k , for a NACA-0012 airfoil, is presented, based on the results of Gregory and O'Reilly ^[23]. In Figure (A- 2) similar results for a NACA-64A006 airfoil are presented, based on the results of McCullough and Gault ^[24]. The results for the two airfoils indicate that at low values of the lift coefficient, the value of k is somewhat higher than the theoretical value of 0.5 . As the angle of attack increases and approaches stall, the value of k increases. The increase in k is more pronounced in the case of NACA 64A006.

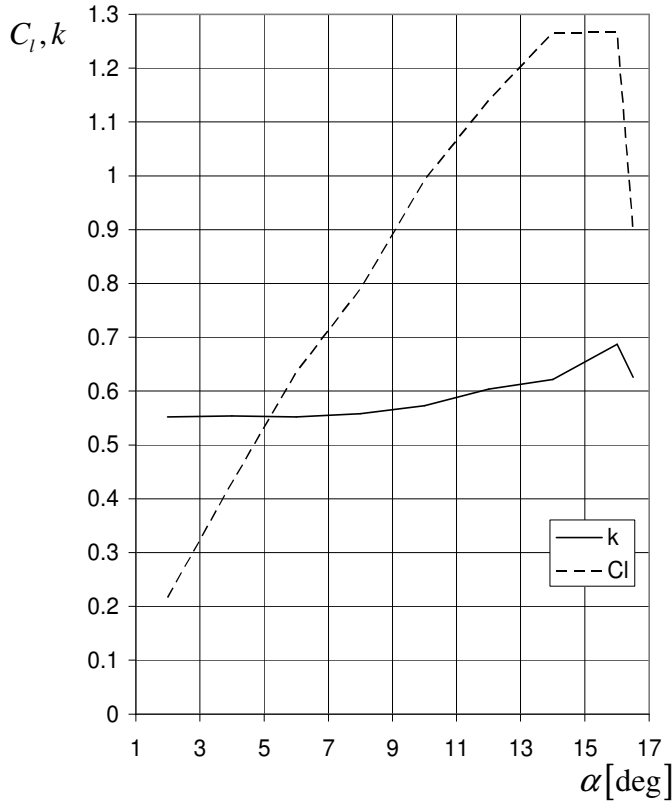


Figure (A- 1): The lift coefficient and value of k for a NACA-0012 airfoil as a function of the angle of attack, $M = 0.16, Re = 2.88 \cdot 10^6$ ^[23]

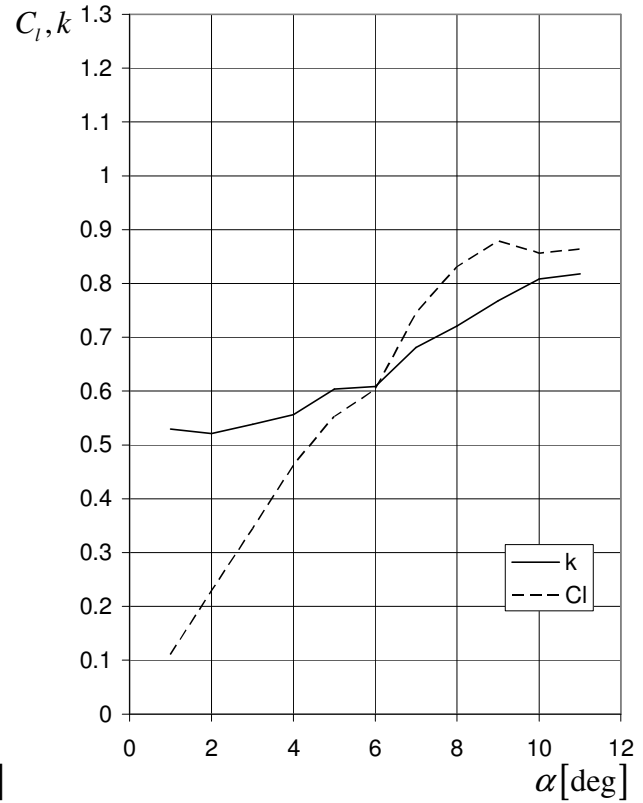


Figure (A- 2): The lift coefficient and value of k for a NACA-64A006 airfoil as a function of the angle of attack, $M = 0.17, Re = 5.8 \cdot 10^6$ ^[24]

APPENDIX B. THE INDUCED VELOCITY DUE TO A PLANNAR AXISYMMETRIC DISTRIBUTION OF SINKS

(r, ψ, z) is a polar system of coordinates. There is an axisymmetric distribution of sinks at the plane $z=0$. The intensity of the sinks distribution, per unit area of the plane, is $\gamma(r)$. The field of the induced velocities is symmetric about the plane $z=0$ and axisymmetric about z .

The radial and axial components of the induced velocities are, $u_r(r, z)$ and $u_z(r, z)$, respectively:

$$u_z(r, z) = -\frac{z}{2 \cdot \pi} \cdot \int_{r'=0}^{r' \rightarrow \infty} \gamma(r') \cdot r' \cdot A(r, z, r') \cdot dr' \quad (\text{B- 1a})$$

$$u_r(r, z) = -\frac{1}{2 \cdot \pi} \cdot \int_{r'=0}^{r' \rightarrow \infty} \gamma(r') \cdot r' \cdot [r \cdot A(r, z, r') - r' \cdot B(r, z, r')] \cdot dr' \quad (\text{B- 1b})$$

where $A(r, z, r')$ and $B(r, z, r')$ are:

$$A(r, z, r') = \int_{\psi'=0}^{\psi'=\pi} \frac{d\psi'}{(r^2 + r'^2 - 2 \cdot r \cdot r' \cdot \cos \psi' + z^2)^{\frac{3}{2}}} \quad (\text{B- 2a})$$

$$B(r, z, r') = \int_{\psi'=0}^{\psi'=\pi} \frac{\cos \psi' \cdot d\psi'}{(r^2 + r'^2 - 2 \cdot r \cdot r' \cdot \cos \psi' + z^2)^{\frac{3}{2}}} \quad (\text{B- 2b})$$

Integration of the last two equations^[25], results in:

$$A(r, z, r') = \frac{2}{[(r-r')^2 + z^2] \cdot \sqrt{(r+r')^2 + z^2}} \cdot E(\kappa) \quad (\text{B- 3a})$$

$$B(r, z, r') = \frac{r^2 + r'^2 + z^2}{r \cdot r' \cdot [(r-r')^2 + z^2] \cdot \sqrt{(r+r')^2 + z^2}} \cdot E(\kappa) - \frac{1}{r \cdot r' \cdot \sqrt{(r+r')^2 + z^2}} \cdot K(\kappa) \quad (\text{B- 3b})$$

Where:

$$\kappa = 2 \cdot \sqrt{\frac{r \cdot r'}{(r+r')^2 + z^2}} \quad (\text{B- 4})$$

$K(\kappa)$ and $E(\kappa)$ are complete elliptic integrals of the first kind and the second kind, respectively

Equations (B- 3a,b) are substituted into Equations (B- 1a,b) and solved numerically. The difficulty of the integration involves a singularity for the case $z \rightarrow 0$ and $r' \rightarrow r$. This

singularity will be dealt with in what follows. Because of the symmetry about the $z=0$ plane, the derivation will be continued for the case $z<0$.

According to Equation (B- 1a), since the integral is multiply by z , the contribution to $u_z(r,0^-)$ is confined to the neighborhood of r , namely $r' \rightarrow r$. Thus:

$$u_z(r,0^-) = \lim_{z \rightarrow 0^-} \left[-\frac{z}{2 \cdot \pi} \cdot \int_{r'=r-\varepsilon}^{r'=r+\varepsilon} \gamma(r') \cdot r' \cdot A(r, z, r') \cdot dr' \right] \quad (\text{B- 5})$$

where ε is a small parameter.

The integral of (B- 5) is solved using the following transformation:

$$\begin{aligned} t &= r' - r \\ dt &= dr' \end{aligned} \quad (\text{B- 6})$$

The elliptic integral of the first kind is replaced by the first two terms of its series expansion ^[25]:

$$E(\kappa) \cong 1 - \frac{(\kappa')^2}{2} \cdot \ln(\kappa') \quad (\text{B- 7})$$

where κ' is:

$$\kappa' = \sqrt{1 - \kappa^2} \quad (\text{B- 8})$$

Substituting Equations (B- 7) and (B- 6) into equation (B- 5), results in:

$$u_z(r,0^-) = \lim_{z \rightarrow 0^-} \left[-\frac{z}{2 \cdot r \cdot \pi} \cdot \int_{r'=r-\varepsilon}^{r'=r+\varepsilon} \frac{\gamma(r) \cdot r \cdot E(1) + O(t)}{t^2 + z^2} \cdot dt \right] = \frac{\gamma(r)}{2} \quad (\text{B- 9})$$

The radial component of the induced velocity for $z \rightarrow 0^-$, $u_r(r,0^-)$, becomes:

$$\begin{aligned} u_r(r, z) &= -\frac{1}{2 \cdot \pi} \cdot \int_{r'=0}^{r'=r-\varepsilon} \gamma(r') \cdot r' \cdot [r \cdot A(r, z, r') - r' \cdot B(r, z, r')] \cdot dr' - \\ &\quad -\frac{1}{2 \cdot \pi} \cdot \int_{r'=r+\varepsilon}^{r' \rightarrow \infty} \gamma(r') \cdot r' \cdot [r \cdot A(r, z, r') - r' \cdot B(r, z, r')] \cdot dr' + I(r, \varepsilon) \end{aligned} \quad (\text{B- 10})$$

The singularity appears in the integral, $I(r, \varepsilon)$:

$$I(r, \varepsilon) = -\frac{1}{2 \cdot \pi} \cdot \int_{r'=r-\varepsilon}^{r'=r+\varepsilon} \gamma(r') \cdot r' \cdot [r \cdot A(r, z, r') - r' \cdot B(r, z, r')] \cdot dr' \quad (\text{B- 11})$$

Substituting Equation (B- 6) into Equation (B- 11) leads to the following expression:

$$I(r, \varepsilon) = -\lim_{\substack{z \rightarrow 0^+ \\ t \rightarrow 0}} \frac{1}{\pi} \cdot \int_{t=-\varepsilon}^{t=\varepsilon} G_1(r, t, z) \cdot E[\kappa(r, t, z)] \cdot dt \quad (\text{B- 12})$$

$$- \lim_{\substack{z \rightarrow 0^+ \\ t \rightarrow 0}} \frac{1}{2 \cdot \pi \cdot r} \cdot \int_{t=-\varepsilon}^{t=\varepsilon} G_2(r, t, z) \cdot \{K[\kappa(r, t, z)] - E[\kappa(r, t, z)]\} \cdot dt$$

where:

$$\kappa(r, t, z) = 2 \cdot \sqrt{\frac{r^2 + r \cdot t}{4 \cdot r^2 + 4 \cdot r \cdot t + t^2 + z^2}} \quad (\text{B- 13a})$$

$$G_1(r, t, z) = \frac{\gamma(r+t) \cdot (r+t) \cdot t}{(t^2 + z^2) \cdot \sqrt{4 \cdot r^2 + 4 \cdot r \cdot t + t^2 + z^2}} \quad (\text{B- 13b})$$

$$G_2(r, t, z) = \frac{\gamma(r+t) \cdot (r+t)}{\sqrt{4 \cdot r^2 + 4 \cdot r \cdot t + t^2 + z^2}} \quad (\text{B- 13c})$$

A Taylor expansion of $G_1(r, t, z)$ and $G_2(r, t, z)$, as defined by Equations (B- 13b,c), then neglecting high orders of t , lead to the following expressions:

$$G_1(r, t, z) \cong \frac{\gamma(r)}{2} \cdot \frac{t}{t^2 + z^2} + \left[\frac{1}{4} \cdot \frac{\gamma(r)}{r} + \frac{1}{2} \cdot \frac{d\gamma}{dr}(r) \right] \cdot \frac{t^2}{t^2 + z^2} \quad (\text{B- 14a})$$

$$G_2(r, t, z) \cong \frac{\gamma(r)}{2} + \left[\frac{1}{4} \cdot \frac{\gamma(r)}{r} + \frac{1}{2} \cdot \frac{d\gamma}{dr}(r) \right] \cdot t \quad (\text{B- 14b})$$

A series expansion of the complete elliptic integral of the second kind leads to the following approximation^[25]:

$$K(\kappa) \cong \ln 4 - \ln(\kappa') \quad (\text{B- 15})$$

Using Equations (B- 7), (B- 8), (B- 13a), and (B- 15) results in the following approximations for the complete elliptic integrals of the first and second kind, for $z \rightarrow 0^-$ and $r' \rightarrow r$:

$$K(r, t, z) \cong \ln(8 \cdot r) - \frac{1}{2} \cdot \ln(t^2 + z^2) \quad (\text{B- 16a})$$

$$E(r, t, z) \cong 1 - \frac{t^2 + z^2}{16 \cdot r^2} \cdot \ln(t^2 + z^2) \quad (\text{B- 16b})$$

Substitution of Equations (B- 14a,b) and (B- 16a,b) into Equation (B- 12) results in:

$$I(r, \varepsilon) = \lim_{\substack{z \rightarrow 0^- \\ t \rightarrow 0}} \left[\frac{1}{4} \cdot \frac{\gamma(r)}{r} + \frac{1}{2} \cdot \frac{d\gamma}{dr}(r) \right] \cdot \frac{1}{\pi} \cdot \int_{t=-\varepsilon}^{t=\varepsilon} \left[\frac{t^2}{t^2 + z^2} - \frac{t^2}{16 \cdot r^2} \cdot \ln(t^2 + z^2) \right] \cdot dt$$

$$- \lim_{\substack{z \rightarrow 0^- \\ t \rightarrow 0}} \frac{\gamma(r)}{4 \cdot \pi \cdot r} \cdot \int_{t=-\varepsilon}^{t=\varepsilon} \left\{ [\ln(8 \cdot r) - 1] - \frac{1}{2} \cdot \ln(t^2 + z^2) \right\} \cdot dt \quad (\text{B- 17})$$

Carrying out the integrations of the last equation and neglecting higher order terms in ε , leads to the following approximation for $I(r, \varepsilon)$:

$$I(r, \varepsilon) \cong \frac{\varepsilon}{2 \cdot \pi \cdot r} \cdot \left\{ \gamma(r) \cdot [\ln \varepsilon + 1 - \ln(8 \cdot r)] + 2 \cdot \frac{d\gamma}{dr}(r) \cdot r \right\} \quad (\text{B- 18})$$

If ε is small enough, then only the term $[\gamma(r) \cdot \ln \varepsilon]$ inside the large brackets can be retained while neglecting the other much smaller ones. Thus the final expression of the radial component of the induced velocity at the entrance to the disk, $u_r(r, 0^-)$, becomes:

$$u_r(r, 0^-) = \lim_{\varepsilon \rightarrow 0} \left\{ -\frac{1}{2 \cdot \pi} \cdot \int_{r'=0}^{r'=r-\varepsilon} \gamma(r') \cdot r' \cdot [r \cdot A(r, z, r') - r' \cdot B(r, z, r')] \cdot dr' \right.$$

$$- \frac{1}{2 \cdot \pi} \cdot \int_{r'=r+\varepsilon}^{r' \rightarrow \infty} \gamma(r') \cdot r' \cdot [r \cdot A(r, z, r') - r' \cdot B(r, z, r')] \cdot dr' \quad (\text{B- 19})$$

$$\left. + \frac{\gamma(r)}{2 \cdot \pi \cdot r} \cdot \varepsilon \cdot \ln \varepsilon \right\}$$

The procedure of calculating $u_r(r, 0^-)$ is as follows: An initial value of ε is defined and $u_r(r, 0^-)$ is calculated according to Equation (B- 19), where numerical integration is

used to find the values of the first two integrals. Then ε is reduced and $u_r(r, 0^-)$ is calculated again. Those calculations are repeated until predetermined convergence criteria are met. This procedure is very efficient and stable.

APPENDIX C. APPROXIMATION FOR $w_z(r)$ OUTSIDE THE DISK FOR $z=0$

The total mass flow rate through the disk ($0 \leq r \leq R$) is C . For points that are far enough from the disk (and are not located near the wake) the induced velocity components are very close to those induced by a sink of intensity C , namely:

$$v_r(r, z) \cong -\frac{C}{4 \cdot \pi} \cdot \frac{r}{(r^2 + z^2)^{3/2}} \quad (\text{C- 1a})$$

$$v_z(r, z) \cong -\frac{C}{4 \cdot \pi} \cdot \frac{z}{(r^2 + z^2)^{3/2}} \quad (\text{C- 1b})$$

For the case $z \ll r$ and $r > R$, it is possible to describe $w_r(r, z)$ and $w_z(r, z)$ as a series that converges rapidly:

$$v_r(r, z) \cong -\frac{C}{4 \cdot \pi} \cdot \left[\frac{1}{r^2} - \frac{3}{2} \cdot \frac{z^2}{r^4} + \frac{15}{8} \cdot \frac{z^4}{r^6} \dots \right] \quad (\text{C- 2a})$$

$$v_z(r, z) \cong -\frac{C}{4 \cdot \pi} \cdot \left[\frac{z}{r^3} - \frac{3}{2} \cdot \frac{z^3}{r^5} + \frac{15}{8} \cdot \frac{z^5}{r^7} \dots \right] \quad (\text{C- 2b})$$

The purpose now is to change Equations (C- 2a,b) in such a manner that they will describe the flow field near the edge of the disk, but for large enough values of r ($r \gg R$) and very small values of z , will converge to the expressions (C- 2a,b). Using first order approximation, the expression for $v_z(r, z)$ becomes:

$$v_z(r, z) \cong \frac{w_z(R) \cdot R^4}{r^4} - \frac{C}{4 \cdot \pi} \cdot \frac{z}{(r^2 + z^2)^{3/2}} \quad \text{for } r \geq R \quad (\text{C- 3})$$

The last expression converges to Equation (C- 2b) for large enough values of r . On the other end it results in a continuity in the value of $v_z(r, z)$ for $r=R$ and $z=0$.

REFERENCE

- [1] W.J.M. Rankine, and W.M. Froude, "On the mechanical principles of the action of propellers", Transactions of the Institution of Naval Architects, Vol. 6, April 1865, pp. 13-39
- [2] J.H. Horlock, "Actuator disk theory", McGraw-Hill, Inc., 1978
- [3] H. Glauert, "Airplane propellers" in "Aerodynamic Theory" (Vol. 4, Division L), F.W. Durand, (Ed.), New York, Dover, 1963.
- [4] D.J. Sharpe, "A general momentum theory applied to an energy-extracting actuator disk", Wind Energy, Vol.7, 2004, pp. 177-188
- [5] D. Thoma, "Grundsatzliches zur einfachen Strahltheorie der Schraube", Zeitschrift für Flugtechnik und Motorluftschiffahrt, Vol. 16, 1925, pp. 206-208
- [6] P.M. Goorjian, "An invalid equation in the general momentum theory of the actuator disk", AIAA Journal, Vol. 10, No. 4, April 1972
- [7] A. Rauh, and W. Seelert, "The Betz Optimum Efficiency for Windmills", vol. 17, no. 1, 1984, pp. 15-23.
- [8] G.A.M. Van Kuik, "On the limitations of Froude's actuator disk concept", Ph.D. Thesis, Technical University of Eindhoven, 1991
- [9] G.A.M. Van Kuik, "On the revision of the actuator disk momentum theory", Wind Engineering, Vol. 15, No. 5, 1991 pp. 276-289
- [10] G.A.M. Van Kuik, "An inconsistency in the actuator disk momentum theory", Wind Energy, Vol. 7, 2003, pp. 9-19
- [11] P.R. Spalart, "On the simple actuator disk", J. of Fluid Mechanics, Vol. 494, 2003, pp.399-405
- [12] S.L. Bragg, and W.R. Hawthorne, "Some exact solutions of the flow through annular cascade actuator disks", J. of the Aeronautical Sciences, Vol. 17, 1950, pp.243-249
- [13] T.Y. Wu, "Flow through a heavily loaded actuator disk", Schiffstechnik, Vol. 9, No. 47, 1962, pp. 134-138
- [14] G.R. Hough, and D.E. Ordway, "The generalized actuator disk", Developments in Theoretical Applied Mechanics, in the proceedings of the Second South Eastern Conference on Theoretical and Applied Technology, Atlanta, 1964, pp. 317-336

- [15] M.D. Greenberg, and S.R. Powers, “Nonlinear actuator disk theory and flow field calculations including nonuniform loading” NASA CR-1672, 1970
- [16] M.D. Greenberg, “Nonlinear actuator disk theory”, Z. Flugwiss, Vol. 20, no. 3, 1972, pp.9-98
- [17] G.H. Schmidt, and J.A. Sparenberg, “ On the edge singularity of an actuator disk with large constant normal load”, J. of Ship Research, vol. 21, No. 2, 1977, pp.125-131
- [18] A.M. Van der Spek, “linear and non-linear theories of flow through an actuator disk”, Report R-803-A, Department of Physics, Technical University of Eindhoven, 1986
- [19] J.T. Conway, “Analytical solutions for the actuator disk with variable radial distribution of load”, Journal of Fluid Mechanics, Vol. 297, 1995, pp. 327-355
- [20] J.T. Conway, “Exact actuator disk solutions for non-uniform heavy loading and slipstream contraction”, Journal of fluid Mechanics, Vol. 365, 1998, pp. 235-267
- [21] J.A. Landgrebe, “An analytical and experimental investigation of helicopter rotor hover performance and wake geometry characteristics”, USAAMRDL Technical Report 71-24, June 1971
- [22] K. Karamcheti, “Principles of ideal-fluid aerodynamics”, John Wiley and Sons, 1966
- [23] N. Gregory, C.L. O’Reilly, “Low speed aerodynamic characteristics of NACA 0012 aerofoil section, including the effects of upper-surface roughness simulating hoar-frost”, R&M 3762, January, 1970
- [24] B.G. McCullough, and E.D. Gault, “Examples of three representative types of airfoil-section stall at low speed”, NACA TN 2502, September 1951
- [25] L.S. Gradshteyn, and I.M. Ryzhik, “Table of integrals, series, and products”, Academic Press, 1980